

# Galaxy Peculiar Velocities From Large-Scale Supernova Surveys as a Dark Energy Probe

Suman Bhattacharya

*T-2, Theoretical Division, Los Alamos National Laboratory, Los Alamos, NM 87545\**

Arthur Kosowsky, Jeffrey A. Newman, and Andrew R. Zentner

*Department of Physics and Astronomy, University of Pittsburgh, Pittsburgh, PA 15260*

Upcoming imaging surveys such as the Large Synoptic Survey Telescope will repeatedly scan large areas of sky and have the potential to yield million-supernova catalogs. Type Ia supernovae are excellent standard candles and will provide distance measures that suffice to detect mean pairwise velocities of their host galaxies. We show that when combining these distance measures with photometric redshifts for either the supernovae or their host galaxies, the mean pairwise velocities of the host galaxies will provide a dark energy probe which is competitive with other widely discussed methods. Adding information from this test to type Ia supernova photometric luminosity distances from the same experiment, plus the cosmic microwave background power spectrum from the Planck satellite, improves the Dark Energy Task Force Figure of Merit by a factor of 1.8. Pairwise velocity measurements require no additional observational effort beyond that required to perform the traditional supernova luminosity distance test, but may provide complementary constraints on dark energy parameters and the nature of gravity. Incorporating additional spectroscopic redshift follow-up observations could provide important dark energy constraints from pairwise velocities alone. Mean pairwise velocities are much less sensitive to systematic redshift errors than the luminosity distance test or weak lensing techniques, and also are only mildly affected by systematic evolution of supernova luminosity.

PACS numbers: 98.62.Py, 98.80.-k, 95.36.+x, 97.60.Bw

## I. INTRODUCTION

Measurements of the distance–redshift relation of type Ia supernovae (SNeIa) firmly established contemporary accelerated cosmological expansion [1, 2] and SNIa distances remain one of the most promising probes of dark energy. To determine whether the accelerated cosmological expansion is caused by an ubiquitous dark energy or large-scale deviations from general relativity, it is necessary to measure both the expansion of the universe and the dynamics of the structure formation [3–14]. The SNIa luminosity distance test provides information about the expansion rate of the universe, but does not provide information on structure formation (though SNIa magnifications may achieve this in the future, see Refs. [15–17]). Peculiar velocities are related to densities through a continuity equation, so peculiar velocity statistics provide one avenue to study the growth of cosmic structure (e.g., [18]). The most well-explored option for probing the peculiar velocity field is via redshift-space distortions imprinted on the galaxy power spectrum (e.g., [19–21]). Peculiar velocities may be detectable with future microwave experiments via the kinetic Sunyaev-Zeldovich effect [22–24] and from large samples of SNeIa with spectroscopic redshifts [25]. In this paper, we examine the possibility of utilizing the mean pairwise velocity statistic, measured from SNeIa in a large photometric survey, to constrain dark energy.

Two well-studied statistics derivable from a sample of line-of-sight peculiar velocities are the *velocity correlation function* and the *mean pairwise velocity* [26, 27]. The former is a two-point statistic expressing correlations in the peculiar velocities of objects as a function of their separation. The mean pairwise velocity is a measure of the typical relative velocity of objects at a given separation. Peculiar velocities are sensitive to both the rate of structure growth in the universe and the rate of expansion of the universe. Therefore, peculiar velocity measurements on cosmological scales may constrain the dark energy that drives cosmological acceleration and quenches late-time structure growth.

Traditionally, the bulk flow velocity has been measured by coupling measured galaxy redshifts with local distance indicators such as the fundamental plane of early-type galaxies [28, 29], the Tully-Fisher relation [30–32], or surface brightness fluctuations [33]. More recent studies [34–36] have measured significant bulk flows on scales of 100 Mpc. Radial velocity measurements have been used to reconstruct the velocity and density fields [37]. Reconstruction

---

\*Electronic address: sumanb@lanl.gov

methods provide a way to test the gravitational instability theory and to measure the bias between the galaxy and mass density fields. Such studies are limited to the relatively local Hubble flow ( $z \lesssim 0.1$ ), primarily because a constant fractional error in distance corresponds to a larger velocity interval at higher redshifts, an error that eventually overcomes the signal.

Type Ia supernovae, in contrast, are well-calibrated standard candles, and at cosmological distances SNeIa are more reliable distance indicators than those previously used for measuring peculiar velocities. Indeed, the dipole and quadrupole moments of the local bulk flow velocity have been measured to higher precision with the current data set of a few hundred SNeIa than with reconstructions based upon catalogs of many thousands of galaxies [25].

SNeIa that are physically near each other exhibit coherent motion as they are influenced by correlated density structures. Therefore, the errors in the luminosity distance measurements of pairs of SNeIa should be correlated at low redshift ( $z \lesssim 0.1$ ). Ignoring this correlation can lead to systematic biases in the determination of dark energy parameters [38–40]. Alternatively, one can treat these correlated shifts in luminosity distance as “signal,” because peculiar velocities depend upon cosmological parameters. This signal has led to useful, independent constraints on the low-redshift normalization of the matter power spectrum,  $\sigma_8$ , and the total matter density,  $\Omega_m$  [41, 42]. Unfortunately, direct measurements of the velocity correlation remain limited to relatively low redshifts. Even in an optimistic scenario of measurements of one million SNeIa, all with full spectroscopic follow-up, the velocity correlation can only be measured to a redshift of  $z \simeq 0.5$  [11].

In contrast to peculiar velocity correlation measurements, mean pairwise velocity is a linear statistic so its errors vary more mildly with redshift. In this study, we show that it will be possible to obtain interesting cosmological information from mean pairwise velocities to a redshift of  $z = 0.9$  in a large photometric survey of SNeIa, such as that planned for the Large Synoptic Survey Telescope (LSST) which is anticipated to increase dramatically our current catalog of SNeIa, by a factor of nearly 1000. We demonstrate that such a measurement can provide dark energy constraints that complement luminosity distance measurements under optimistic, but reasonable, assumptions. The constraints from mean pairwise velocities are also useful because they may be estimated with relatively little additional observational effort beyond that already required to use SNeIa to map luminosity distance or to detect cosmic lensing magnification [17]. We find that combining the mean pairwise velocity measurements with distance measurements of SNeIa will sharpen constraints on the dark energy parameters compared to those inferred from luminosity distances alone. In particular, mean pairwise velocity constraints can improve the dark energy Figure of Merit from SNeIa as defined by the Dark Energy Task Force [43] (DETF) by a factor of 1.8. We additionally demonstrate that mean pairwise velocities, being a differential statistic, are potentially much less sensitive to systematic errors than other commonly considered observational techniques. Ultimately, this property may make mean pairwise velocities one of the most practically useful probes of dark energy.

Following the DETF, we describe the dark energy in terms of three phenomenological parameters: its current energy density  $\Omega_\Lambda$  and two parameters describing the redshift evolution of its equation of state,  $w_0$  and  $w_a$ , such that  $w(a) = w_0 + (1 - a)w_a$ . The additional cosmological parameters upon which the velocity field depends are the large-scale normalization of the matter power spectrum  $\Delta_\zeta$ , the power-law index of the primordial power spectrum  $n_S$ , the Hubble parameter  $h$ , the curvature of the universe  $\Omega_k$ , and the present-day matter density  $\Omega_m$ . In addition, we treat the photometric redshift (photo- $z$ ) dispersion,  $\sigma_z$ , as a free parameter with priors. We label our set of parameters  $\mathbf{p}$ . We consider a fiducial cosmological model similar to the WMAP 5-year results [44]:  $\Delta_\zeta = 2.0 \times 10^{-9}$ ,  $n_S = 0.95$ ,  $h = 0.71$ ,  $\Omega_k = 0$ ,  $\Omega_m = 0.25$ ,  $\Omega_\Lambda = 0.75$ ,  $w_0 = -1$ , and  $w_a = 0$ .

The paper is organized as follows. In Section II, we describe our assumed SNIa survey specifications and review the estimation of supernova line-of-sight peculiar velocities from observed supernova brightnesses and redshifts. Section III describes a halo model calculation of the mean pairwise velocity as a function of cosmological parameters. Sections IV and V quantify various sources of systematic and statistical errors that impact SNIa pairwise velocity measurements respectively. We present our results for dark energy parameter constraints in Section VI, using two different sets of prior constraints. We also derive limits on systematic effects that must be obtained to have the resulting parameter bias be smaller than the calculated statistical errors. In Section VII, we summarize the kinds of observational efforts required to meet the prospects outlined in this paper, along with a brief discussion of the systematic error properties of mean pairwise velocities compared to other dark energy probes.

## II. LARGE-AREA PHOTOMETRIC SUPERNOVA SURVEYS

Forthcoming large-scale imaging surveys such as LSST or the Panoramic Survey Telescope and Rapid Response System (PanSTARRS) [45–47] will discover  $10^4$  to  $10^6$  SNeIa. These SNeIa may be observed with broadband photometry with exposures spaced several days apart. To infer cosmological parameters from peculiar velocities, reliable distance measurements are needed. These will likely be obtained from a well-characterized subset of the supernovae discovered by any survey. The particular characteristics of this subset depend upon survey strategy and are difficult

to anticipate.

For ease of comparison with published studies, we adopt survey specifications similar to what may be achieved with a survey similar to LSST. We assume a total of  $3 \times 10^5$  SNeIa out to  $z = 1.2$ , collected over a dedicated supernova survey region of 300 square degrees; this corresponds to a SNIa surface density of  $1000 \text{ deg}^{-2}$ . This number density corresponds to the “d2k” survey described in [48] and such a dedicated survey may be undertaken as part of the science goals of the LSST [47]. We assume redshifts estimated using broadband photometry with a redshift-dependent, normally-distributed error of  $\sigma_z = \sigma_{z0}(1+z)$ . DETF specifies an error range of  $\sigma_{z0} = 0.01$  for an optimistic scenario to  $\sigma_{z0} = 0.05$  for a pessimistic scenario; in our parameter forecasts, we allow  $\sigma_{z0}$  to vary along with the cosmological parameters. Following Zhan et al. [48], we model the SNeIa redshift distribution as

$$\frac{d^3 n}{d\Omega dz dt} \propto \begin{cases} \exp(3.12z^{2.1}) - 1, & z \leq 0.5, \\ (\exp(3.12z^{2.1}) - 1) \exp(-12.2(z - 0.5)^2), & z > 0.5. \end{cases} \quad (1)$$

To the extent that SNeIa are standardizable candles, photometric observations will yield a distance modulus  $\mu$  and a luminosity distance  $d_L$  via the usual relation

$$\mu = 2.17 \ln \left( \frac{d_L}{\text{Mpc}} \right) + 25. \quad (2)$$

The luminosity distance is obtained from the cosmological redshift  $z$  via the definition

$$d_L(z) = (1+z)d_C(z) = (1+z)c \int_0^z \frac{dz'}{H(z')}, \quad (3)$$

where  $d_C(z)$  is the comoving line-of-sight distance to a galaxy at redshift  $z$ ,  $H(z)$  is the Hubble parameter as a function of redshift, and a geometrically flat universe has been assumed in the second equality. The evolution of the Hubble parameter, and thus the luminosity distance, depends on the assumed cosmological model. For a given supernova, its measured redshift is the difference between its cosmological redshift and the additional Doppler shift due to its line-of-sight velocity,

$$z_{\text{meas}} = z(\mu) - \frac{v_{\text{los}}}{c}(1+z(\mu)), \quad (4)$$

where its cosmological redshift  $z(\mu)$  can be obtained from its observed luminosity by inverting Eqs. (2) and (3). The factor of  $(1+z)$  in Eq. (4) accounts for the cosmological redshift between the rest frame and the observation frame. For a given supernova with observed redshift and luminosity, its line-of-sight velocity can be obtained by rearranging Eq. (4) into

$$v_{\text{los}} = \frac{cz(\mu) - cz_{\text{meas}}}{1+z_{\text{meas}}}, \quad (5)$$

where we have replaced  $z(\mu)$  by  $z_{\text{meas}}$  in the denominator, which will always be a good approximation for objects at cosmological distances where the first term in Eq. (4) is large compared to the second term.

Traditional peculiar velocity estimates using other standard candles at cosmological distances have been hampered by errors in distance estimates, which propagate into errors in  $z(\mu)$ . For a galaxy with cosmological redshift  $z = 0.03$ , a 10% error in distance corresponds to an error in inferred cosmological redshift equivalent to a peculiar velocity of 1000 km/s, with the size of the error increasing proportional to redshift for  $z \leq 1$ . Large-area supernova surveys offer two main advantages. First, supernovae are bright enough and good enough standard candles to provide convenient distance estimators out to  $z = 1$  and beyond. Second, the anticipated large number of supernovae hold the promise of determining average distances far more precisely than individual distances, allowing precise determination of average velocity statistics from large catalogs of supernovae. Of course, realizing this promise requires controlling systematic errors in both distance and redshift observations to a high level, so that averages over large ensembles of SNeIa reflect the actual velocity statistic. Both systematic and statistical errors will be considered following the next Section, which outlines the application of the mean pairwise velocity statistic to supernova surveys.

### III. MEAN PAIRWISE PECULIAR VELOCITY

The mean pairwise velocity  $v(r, a)$  at a comoving separation  $r$  and scale factor  $a = 1/(1+z)$  is the average over all pairs at a fixed comoving separation of the relative peculiar velocity of the two galaxies projected along the line

joining them. That is,

$$v(r, a) = \frac{1}{N(r)} \sum_{i \neq j} (\mathbf{v}_i - \mathbf{v}_j) \cdot \hat{\mathbf{r}}, \quad (6)$$

where  $\mathbf{v}_i$  is the peculiar velocity of supernova  $i$  and  $\hat{\mathbf{r}}$  is the unit vector in the direction of the separation of the two objects. The sum is over  $N(r)$  pairs at a given comoving separation  $r$ . (Note that the quantity which we write throughout this paper as “ $v(r, a)$ ” is commonly written in the literature as “ $v_{ij}(r, a)$ ” or “ $v_{12}(r, a)$ .” We use this notation to avoid potential confusion with subscript labels for individual galaxies that we use below.)

The mean pairwise velocity for dark matter particles may be derived using the pair conservation equation [49]. However for galaxies, the pair conservation equation needs to be modified to account for evolution [27]. The resulting mean pairwise velocity for SNIa host galaxies with a comoving separation  $r$  at a mean scale factor  $a$  (assuming that the redshift difference between the two galaxies corresponds to a scale factor difference much smaller than  $a$ ) can be written

$$v(r, a) = -\frac{2}{3} H(a) a \frac{d \ln D_a}{d \ln a} b_{\text{gal}}(a) \frac{r \bar{\xi}^{\text{dm}}(r, a)}{1 + \xi^{\text{gal}}(r, a)}, \quad (7)$$

where

$$\xi^{\text{dm}}(r, a) = \frac{D_a^2}{2\pi^2 r} \int_0^\infty dk k \sin(kr) P(k) \quad (8)$$

is the dark matter two-point correlation function,  $P(k)$  is the dark matter power spectrum at wavenumber  $k$ ,  $H(a)$  is the Hubble parameter at a given redshift, and  $D_a$  is the linear growth factor as a function of time, normalized so that  $D_a = 1$  at  $z = 0$ . We also define the dark matter correlation function averaged over separations less than  $r$  to be

$$\bar{\xi}^{\text{dm}}(r, a) = \frac{3}{r^3} \int_0^r dr' r'^2 \xi^{\text{dm}}(r', a). \quad (9)$$

We are interested in the large-scale limit, so we model the correlation function of supernova host galaxies using a deterministic linear bias relative to the dark matter  $b_{\text{gal}}(z)$ , defined by

$$\xi^{\text{gal}}(r, a) = b_{\text{gal}}^2(z) \xi^{\text{dm}}(r, a). \quad (10)$$

The bias  $b_{\text{gal}}(z)$  in general varies with the galaxy separation, a variety of galaxy properties, and redshift [50]. In the large-scale limit, scale-independent bias is a fairly good assumption. Following Ref. [48], we model  $b_{\text{gal}}(z)$  as  $b_{\text{gal}}(z) = 1.0 + 0.6z$  to obtain the fiducial value of the galaxy bias as a function of redshift.

With future photometric surveys potentially detecting more than a billion galaxies, we can expect that the correlation function of samples of galaxies matching the SN hosts can be measured to percent-level accuracy or better. Thus the uncertainty in  $b_{\text{gal}}$  will primarily be due to uncertainty in the cosmological parameters affecting the dark matter correlation function. We express  $b_{\text{gal}}$  in terms of the galaxy and predicted dark matter correlation functions, and use this bias value in Eq. (7).

Only the line-of-sight component of the velocity can be obtained from observations, while the mean pairwise velocity involves all three directional components of the velocity. We use the estimator for the mean pairwise velocity given a data set of line-of-sight velocities developed in Ref. [26]. Consider two galaxies  $i$  and  $j$  at comoving positions  $\mathbf{r}_i$  and  $\mathbf{r}_j$  moving with peculiar velocities  $\mathbf{v}_i$  and  $\mathbf{v}_j$ . The radial component of velocities can be written as  $v_i^r = \hat{\mathbf{r}}_i \cdot \mathbf{v}_i$  and  $v_j^r = \hat{\mathbf{r}}_j \cdot \mathbf{v}_j$ . Then an estimate for the pairwise velocity of the two galaxies  $v_{ij}^{\text{est}}$  is defined by  $\langle v_i^r - v_j^r \rangle = v_{ij}^{\text{est}} \hat{\mathbf{r}} \cdot (\hat{\mathbf{r}}_i + \hat{\mathbf{r}}_j)/2$ , where  $\hat{\mathbf{r}}$  is the unit vector along the line joining the two galaxies. If we now consider a catalog of line-of-sight galaxy velocities, minimizing  $\chi^2$  between the actual pairwise velocities and the estimate of the pairwise velocity at a given separation  $r$  gives an estimator for the pairwise velocity Eq. (7) based on the catalog,

$$v^{\text{est}}(r, a) = \frac{\sum_{\text{pairs}} (v_i^r - v_j^r) p_{ij}}{\sum_{\text{pairs}} p_{ij}^2}, \quad (11)$$

where the sums are over all pairs  $i \neq j$  of galaxies at comoving separation  $r$  and  $p_{ij} = \hat{\mathbf{r}} \cdot (\hat{\mathbf{r}}_i + \hat{\mathbf{r}}_j)/2$ . Note that this form for the projection tensor  $p_{ij}$  is applicable in the flat-sky limit and breaks down for large angular separations; in particular it is zero if the two galaxies are in opposite sky directions. In this paper, we consider a model supernova survey of 300 square degrees in a compact sky region, and the  $p_{ij}$  expression given here is always valid. To extend the results here to a full-sky survey, or to survey patches which are separated by large angles, a more complicated

projection tensor must be used. The derivation is not conceptually difficult, but this will be deferred to future work giving more detailed estimates of signal-to-noise ratios for particular observing strategies.

Equation (11) is a function of the separation  $r$  between the two galaxies. To measure this distance, we must use the estimated locations of each galaxy; this is subject to errors which will be quantified in the next Section. The separation that is measured directly is the angle between two galaxies on the sky. This angle can be converted to the transverse component of the distance between the two galaxies using the angular diameter distances corresponding to their redshifts.

The expression in Eq. (11) is a very simple estimator which weights all pairs of velocities uniformly. A more careful analysis of real data would use, for example, a signal-to-noise weighting in the sum. This is not a major correction to the analysis in this paper, as we limit the sums in Eq. (11) to pairs with separations smaller than 100 Mpc; at larger separations the signal becomes small. In principle, a signal-to-noise weighting can squeeze more information out of the data, using pairs with larger separations, but it does not qualitatively change our results. Our estimator is accurate, as we have shown explicitly in Fig. 4 of Ref. [23], but suboptimal; an optimal estimator will somewhat improve the constraining capability of a velocity survey compared to the analysis here, so our estimator is conservative.

As we discuss further in Section IV and Section VI, we can mitigate the influence of systematic redshift errors by considering a related projected statistic, where the mean pairwise velocity is taken as a function of the angular separation of the two galaxies rather than as a function of their three-dimensional separation. This is given by

$$\tilde{v}(\theta, a) = \int_0^{\pi_{\max}} d\pi_t P(\pi_t|\theta, a) v(r, a), \quad (12)$$

where the line-of-sight comoving separation  $\pi_t = d_C(a_2) - d_C(a_1)$  and  $P(\pi_t|\theta, a)$  is the probability that a pair has line-of-sight separation  $\pi_t$  given that it has an angular separation on the sky  $\theta$ . We can write the three-dimensional separation  $r$  in terms of the angular separation  $\theta$  and  $\pi_t$  as

$$r = \sqrt{\theta^2 d_M(a)^2 + \pi_t^2}, \quad (13)$$

where

$$d_M(a) = \begin{cases} cH_0^{-1}\Omega_k^{-1/2} \sinh \left[ \Omega_k^{1/2} d_C(a)/(cH_0^{-1}) \right], & \Omega_k > 0 \\ d_C(a), & \Omega_k = 0 \\ cH_0^{-1}|\Omega_k|^{-1/2} \sin \left[ |\Omega_k|^{1/2} d_C(a)/(cH_0^{-1}) \right], & \Omega_k < 0 \end{cases} \quad (14)$$

is the transverse comoving distance to scale factor  $a$ ; here  $\Omega_k$  is the effective curvature density,  $\Omega_k = 1 - \Omega_m - \Omega_\Lambda$  (see Ref. [51] for a lucid discussion of various distance measures in cosmology). If the redshift difference is small compared to unity,  $\pi_t H(z_1) \approx c(z_2 - z_1)$ , though we compute the separation in full for all pairs. For a spatially flat universe,  $d_M(a) = d_C(a)$ . In our case, we always consider separations with  $r \ll cH_0^{-1}$  since the signal is only significant on these scales. We therefore always have  $d_M(a) \approx d_C(a)$  to good accuracy, and for simplicity we make this assumption throughout the rest of the paper and use comoving distances entirely. We consider pairs of galaxies with line-of-sight comoving separations up to a maximum value  $\pi_{\max}$  (in practice, we will measure redshift-space rather than comoving separations; we consider the impact of this in Section IV A). The probability of a pair having line-of-sight separation  $\pi_t$  given that it has an angular separation on the sky  $\theta$  is

$$P(\pi_t|\theta, a) = \frac{1 + \xi^{\text{gal}}(r, a)}{\int_0^{\pi_{\max}} d\pi_t [1 + \xi^{\text{gal}}(r, a)]} \quad (15)$$

for  $\pi_t < \pi_{\max}$  and  $P(\pi_t|\theta, a) = 0$  for  $\pi_t > \pi_{\max}$ .

An estimator for  $\tilde{v}(\theta, a)$  from line-of-sight velocity data is easily obtained by substituting  $v^{\text{est}}(r, a)$  for  $v(r, a)$  in Eq. (12). To compare with data, we bin this statistic in angular separation and redshift, putting each pair in the redshift bin corresponding to the mean photometric redshift of the two galaxies in the pair. In this manner all pairs are included regardless of binning; we have verified that our results remain similar when modest changes are made to projection and binning schemes. Note a correction for scatter in measured redshifts must also be included, as discussed below in the following Section.

Changing the maximum separation  $\pi_{\max}$  considered in Eq. (12) will modify the signal-to-noise ratio in measuring the projected pairwise velocity. A larger  $\pi_{\max}$  increases the total number of pairs considered, but the signal-to-noise ratio for each pair decreases at larger  $\pi_t$  (as measurement errors remain approximately unchanged but signal strength decreases), so their contribution is small. For the purposes of this paper, we adopt a cutoff of  $\pi_{\max} = 100$  Mpc, which captures the great majority of the pairwise velocity signal. As a test of this effect, we find that including pairs out to

separations two times larger only changes the signal-to-noise in measuring the projected pairwise velocity by around 10%. Based on this, we conclude that including data from pairs with separations larger than 100 Mpc should give only minimal improvements in parameter constraints compared to those presented here. We also impose a minimum separation of 20 Mpc on the pairs we consider, to eliminate any systematic errors related to nonlinear effects. The mean pairwise velocity is a declining function as separation increases from 20 Mpc to 100 Mpc, as shown in Fig. 1; at smaller scales, it turns over and decreases in linear theory.

## IV. SYSTEMATIC ERRORS

### A. Photometric Redshift Errors

Large imaging surveys will detect so many galaxies that it will not be feasible to obtain spectroscopic redshifts for the vast majority. We must settle for photometric redshift estimates determined from the fluxes measured in the various observed bands. These photometric redshifts will be less accurate than spectroscopic redshifts, and may have complex error distributions. Here we consider a measured redshift distribution described by a Gaussian of standard deviation  $\sigma_z$  centered at the true redshift of each object. We neglect a possible photometric redshift bias for two reasons: First, in realistic surveys this bias can be calibrated by comparison with a manageable number of spectroscopic SNIa observations [17, 43, 48]. We emphasize that we utilize a normal distribution for definiteness, but a well-calibrated error distribution is what is necessary to proceed; errors need not be Gaussian in practice. Second, the expected level of photometric redshift bias is likely to be a small effect [52, 53] compared to the systematic errors in estimating distances that we consider below. As a result, we do not explicitly carry a bias through in the equations below, but we will present a test of the impact of a bias in photometric redshifts in Sec. VI.

In contrast, the photo- $z$  dispersion,  $\sigma_z$ , essentially smooths the estimated velocity distribution of the observed sample and propagates scatter into galaxy pair separations. The latter effect can cause not only a scatter in inferred cosmological parameter values, but also a systematic shift, which we calculate here.

The mean pairwise velocity  $v(r, a)$ , given in Eq. (7), assumes that the three-dimensional separation  $r$  between the SNeIa or their host galaxy pairs are known accurately; however, there will be non-negligible errors in observed redshifts. Our simple normal-error model for the distribution of the photometric redshift  $z_p$ , given a true redshift  $z$ , is

$$P(z_p|z, \sigma_z) = \frac{1}{\sqrt{2\pi\sigma_z^2}} \exp[-(z - z_p)^2/(2\sigma_z^2)]. \quad (16)$$

We take the photo- $z$  dispersion to be  $\sigma_z = \sigma_{z0}(1+z)$  with  $\sigma_{z0}$  ranging from 0.01 to 0.05 [6, 43, 48, 52, 53]. We explore the sensitivity of our results to prior knowledge of  $\sigma_{z0}$  in § VI.

Using Eq. (16) and the expression  $H(z_p)\pi_t = c(z_{p2} - z_{p1})$  for the local Hubble expansion about each SNIa, where  $z_{p2} - z_{p1}$  is the photometric redshift difference between a pair of supernovae, we write the probability of obtaining the observed line-of-sight separation  $\pi_{\text{obs}}$  for a given, true comoving line-of-sight separation  $\pi_t$  as

$$P(\pi_{\text{obs}}|\pi_t, \sigma_\pi) = \frac{1}{\sqrt{2\pi\sigma_\pi^2}} \exp[-(\pi_{\text{obs}} - \pi_t)^2/(2\sigma_\pi^2)], \quad (17)$$

where  $\sigma_\pi = \sqrt{2}c\sigma_z/H(z)$  [53]. We assume that the photometric redshifts  $z_p$ , although they include the effects of peculiar motions, give a better measurement of the galaxy line-of-sight separation than the cosmological redshifts  $z(\mu)$ , which must be determined via a distance measurement with uncertainties on the order of 10%; hence the line-of-sight positions of SNeIa are estimated using  $z_p$ . The factor  $\sqrt{2}$  in relating  $\sigma_\pi$  to  $\sigma_z$  accounts for uncertainties in the positions of the two galaxies in a pair, which are added in quadrature. Combining Eqs. (7), (12), and (17), we get an expression for the projected, mean pairwise velocity accounting for a significant dispersion in photometric redshifts,

$$\tilde{v}(\theta, a|\sigma_\pi(a)) = \int_0^{\pi_{\text{max}}} d\pi_t \int_0^\infty d\pi_{\text{obs}} P(\pi_t|\theta, a) P(\pi_{\text{obs}}|\pi_t, \sigma_\pi(a)) v((\theta^2 d_C(a)^2 + \pi_t^2)^{1/2}, a). \quad (18)$$

We propose using this statistic as a cosmological probe. We consider only positive values of  $\pi_t$ , so we count each pair only once. This remains true if in some cases (due to errors)  $\pi_t$  scatters below zero (in which case the separation is positive when the two members of the pair are exchanged).

Both Eq. (17) and the expression for  $\sigma_\pi$  are valid only when  $|z_{p2} - z_{p1}| \ll 1$ ; however, we should always be in this limit. The maximum true separation we consider,  $\pi_{\text{max}} = 100$  Mpc, corresponds to a redshift difference ranging from 0.024 to 0.042 as  $z$  ranges from 0 to 1; photo- $z$  errors will broaden the distribution of separations via a Gaussian

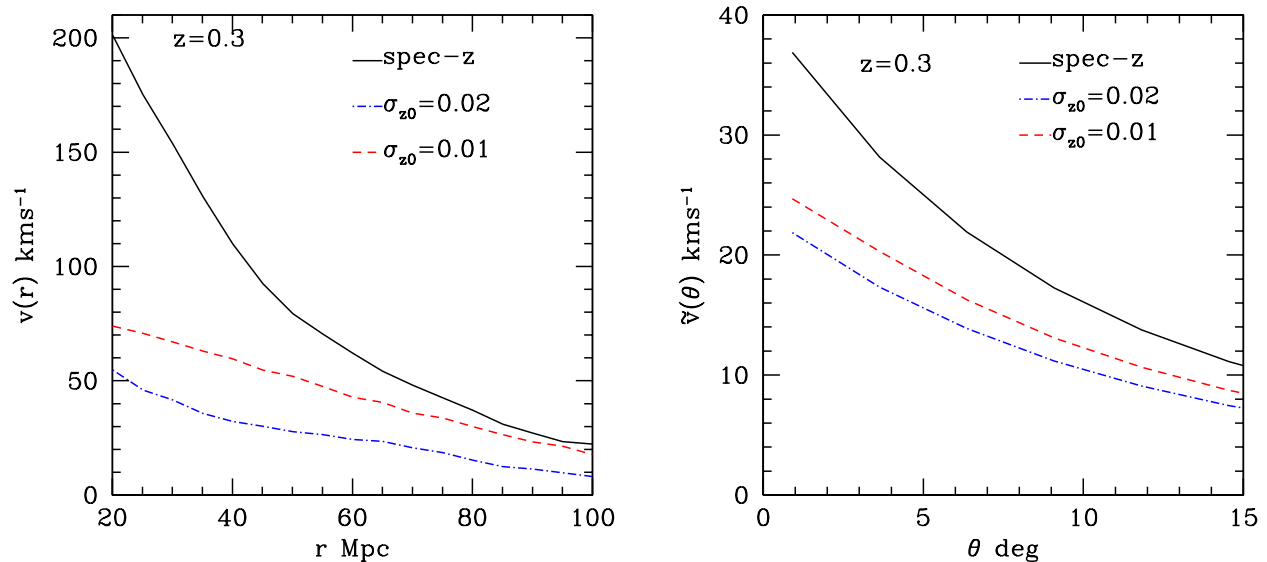


FIG. 1: Effect of photo- $z$  errors on the mean pairwise velocity as a function of the three-dimensional separation  $r$  (left panel) and on the projected mean pairwise velocity as a function of angular separation  $\theta$  (right panel). The solid line represents the spectroscopic sample where the positions of the SNIa host galaxies are known accurately. The dashed line corresponds to a scenario where the dispersion in the photo- $z$  distribution about the true redshift is given by  $\sigma_z = \sigma_{z0}(1+z)$  with  $\sigma_{z0} = 0.01$ , whereas the dot-dashed line represents the case when  $\sigma_{z0} = 0.02$ . Projected statistics vary less with  $\sigma_{z0}$ , so they are less sensitive to systematic errors in this quantity.

kernel with dispersion  $\sigma = \sqrt{2}\sigma_z = \sqrt{2}\sigma_{z0}(1+z)$ , which gives  $\sigma_z = 0.056$  at  $z = 1$  for  $\sigma_{z0} = 0.02$ . To the degree that the assumption of small  $|z_{p2} - z_{p1}|$  is violated, the small distance error induced by this approximation remains negligible, as the pairwise velocity does not vary rapidly on any scales of interest. One additional caveat is that these relations hold only for sufficiently large angular separations, corresponding to comoving separations greater than approximately 5 Mpc, so that nonlinear effects due to velocities within gravitationally bound objects (“fingers of god”) are insignificant.

The left panel of Figure 1 shows the effect of photo- $z$  errors on mean pairwise velocity measurements as a function of three-dimensional separation  $r$ . For a photo- $z$  error  $\sigma_{z0}$  in the range 0.01 to 0.02, the overall amplitude of the mean pairwise velocity is suppressed by a factor of 3 to 4 at separations  $r \leq 50$  Mpc/ $h$  compared to the case where all redshifts are known perfectly. As the separation increases, this suppression becomes less prominent. This is largely because the three-dimensional separations of the SNeIa are uncertain by an amount given by the photo- $z$  error, which may be large compared to the three-dimensional distances when the separation is small. For pairs which are farther apart (and often have distances dominated by their transverse separations), this smearing effect has much less impact. The right panel of Fig. 1 shows the projected mean pairwise velocity as a function of angular separation for different assumed photo- $z$  errors. Note that because of the integration along the line of sight, changing photo- $z$  errors by a factor of two, from  $\sigma_{z0} = 0.01$  to  $\sigma_{z0} = 0.02$ , causes only a 10% to 15% change in the amplitude of the statistic.

## B. Evolution in the Luminosities of Type Ia Supernovae

Evolution in intrinsic SNIa properties is one of the most important potential sources of systematic error that could bias estimates of cosmological parameters from pairwise velocities. For instance, the mean intrinsic luminosity of SNeIa could vary significantly over time. If this were unaccounted for, the inferred distance moduli for supernovae would have a systematic error whose amplitude is a function of redshift. Following Ref. [43], we model an error in the distance modulus  $\mu$  as

$$\mu = \mu_{\text{true}} + \Delta\mu = \mu_{\text{true}} + \mu_L z + \mu_Q z^2, \quad (19)$$

where  $\mu_L$  and  $\mu_Q$  are parameters quantifying the linear and quadratic dependence of the systematic error on redshift. A systematic error in distance modulus propagates into an error in the inferred cosmological redshift  $z(\mu)$  in Eq. (5), while a systematic error in the photometric redshift directly affects  $z_{\text{meas}}$ .

Propagating errors through Eqs. (2) and (3) gives

$$\Delta z = \frac{0.46\Delta\mu(1+z)}{f(z)}, \quad (20)$$

where we define the function

$$f(z) \equiv 1 + \frac{(1+z)^2}{d_L(z)H(z)}. \quad (21)$$

The resulting error in the line-of-sight velocity for a given supernova is

$$\Delta v_{\text{los}} = \frac{0.46c\Delta\mu}{f(z_{\text{meas}})}. \quad (22)$$

Using the measured redshift instead of the cosmological redshift in this expression gives an error on the order of a few percent at redshifts of interest.

This systematic shift can be applied directly to the estimator Eq. (11) to evaluate the impact systematic errors have upon a given supernova velocity catalog. Alternately, we can apply this systematic error to Eq. (6) to get an estimate of the size of the resulting shift in the pairwise velocity statistic. Consider a pair of supernovae with measured redshifts  $z_1$  and  $z_2$ . Each of them has their three-dimensional velocity systematically shifted in the line-of-sight direction by an amount  $\Delta v_{\text{los}}$ ; the component of this shift along the vector connecting the two galaxies is  $\Delta v_{\text{los}}\pi_t/r$  where  $\pi_t$  is their separation along the line of sight and  $r$  is the distance between the galaxies. Their pairwise velocity gets a systematic shift given by

$$\Delta v(r, a) = \frac{c\pi_t}{r} \left( \frac{\Delta z_2}{1+z_2} - \frac{\Delta z_1}{1+z_1} \right) = \frac{0.46c\pi_t}{r} \left( \frac{\Delta\mu_2}{f(z_2)} - \frac{\Delta\mu_1}{f(z_1)} \right) \simeq \frac{0.46H(z_1)\pi_t^2}{f(z_1)r} (\mu_L + 2z_1\mu_Q), \quad (23)$$

where for the last expression we have used the fact that the difference in the second expression is dominated by the difference in distance modulus, rather than the much smaller difference in  $f(z)$ . In replacing both redshifts by  $z_1$  in this expression, we have assumed that the redshift difference for a given pair is small compared to unity, which will be the case for any pair separations for which the mean pairwise velocity is significant. For a given value of  $r$  and  $a = (1+z_1)^{-1}$ , the only quantity which varies between different pairs is the line-of-sight separation term,  $\pi_t^2$ , whose average over random pairs is  $r^2/2$ . Averaging the final expression in Eq. (23) over all pairs with a given separation replace  $\pi_t^2/r$  by  $r/2$  and gives the systematic error in the mean pairwise velocity for pairs with comoving separation  $r$  and mean redshift  $z$  as

$$\Delta v(r, z) = 0.23r \frac{H(z)(\mu_L + 2z\mu_Q)}{f(z)}. \quad (24)$$

For the systematic error in the projected statistic, we substitute Eq. (24) into Eq. (12), which yields

$$\Delta \tilde{v}(\theta, z) = 0.23 \frac{H(z)}{f(z)} (\mu_L + 2\mu_Q z) \int_0^{\pi_{\text{max}}} d\pi_t P(\pi_t|\theta, z) \sqrt{\theta^2 d_C(z)^2 + \pi_t^2}, \quad (25)$$

with  $P(\pi_t|\theta, z)$  given by Eq. (15). This expression is used in Sec. VI to estimate how small this systematic error must be so that it does not dominate the statistical errors in mean pairwise velocity measurements of dark energy parameters.

## V. STATISTICAL ERRORS

The line-of-sight velocity for a supernova is inferred by combining a redshift measurement and a distance estimate obtained from a brightness measurement. Here we assume Gaussian random errors for both the redshift and brightness measurements, and find the resulting statistical error in the mean pairwise velocity. We also give an expression for the sample variance (sometimes referred to as cosmic variance) error in this quantity, which results from the fact that its intrinsic value in the limited volume we probe may not match the universal mean.



### A. Apparent Magnitude and Redshift Errors

For a given supernova, we assume normal errors of  $\sigma_\mu$  and  $\sigma_z$  on the distance modulus and the measured redshift. Propagating through Eq. (5) using Eq. (20) and adding the resulting errors in quadrature gives

$$\delta v_{\text{los}}(z)^2 = \frac{0.21c^2}{f(z)^2} \sigma_\mu^2 + \frac{c^2}{(1+z)^2} \sigma_z^2. \quad (26)$$

In evaluating the first term, we have assumed that  $\sigma_z$  is small compared to  $z_{\text{meas}}$ , which should be a good approximation for photometric redshifts of SNeIa [52, 53]. This allows us to neglect the effect of errors in  $z_{\text{meas}}$  on the value of  $f(z)$ . Note that in actual measurements the errors in photometric redshifts may be significantly non-Gaussian, requiring a more sophisticated treatment; here we explore Gaussian errors to give an approximate guideline for the relevant levels of uncertainty.

Gravitational lensing may increase the dispersion in the measured distance moduli of SNeIa beyond that of intrinsic luminosity scatter and random measurement errors. In the weak lensing limit (convergence  $\kappa \ll 1$ ), the dispersion due to lensing is [16, 17, 54, 55]

$$\sigma_{\text{lens}}^2(z) \approx 1.69 \Omega_m^2 H_0^2 \int_0^z dz' \frac{W^2(z', z)}{H(z)} \int dk k P(k, z'), \quad (27)$$

where  $W(z', z) = H_0 d_A(z') d_A(z', z) / d_A(z)$ ,  $d_A(z)$  is the angular diameter distance to redshift  $z$ , and  $d_A(z', z)$  is the angular diameter distance between redshifts  $z'$  and  $z$ . The quantity  $P(k, z)$  is the matter power spectrum; we evaluate it using the numerical fits of Smith et al. [56]. We thus have a total standard error on the distance modulus for a single supernova composed of three pieces:

$$\sigma_\mu^2 = \sigma_{\text{obs}}^2 + \sigma_{\text{SN}}^2 + \sigma_{\text{lens}}^2, \quad (28)$$

where  $\sigma_{\text{obs}}$  is the random scatter due to measurement noise and  $\sigma_{\text{SN}}$  is the intrinsic scatter in supernova intrinsic luminosity. Where not otherwise specified, we take  $\sigma_{\text{SN}} = 0.1$  independent of redshift, following recent estimates [43], and assume  $\sigma_{\text{obs}} \ll \sigma_{\text{SN}}$ , which should be satisfied for upcoming large surveys like LSST.

To obtain the standard error in the mean pairwise velocity, we begin by assuming that each individual line-of-sight velocity has a normally-distributed error with standard deviation  $\delta v_{\text{los}}$ . Then for any data bin, applying standard propagation of errors to Eq. (11) gives:

$$\delta v^{\text{est}} = \sqrt{2} \delta v_{\text{los}} \left( \sum_{\text{pairs}} p_{ij}^2 \right)^{-1/2}, \quad (29)$$

assuming that fractional errors in the  $p_{ij}$  are modest; we expect this to hold, as these values can be evaluated using redshift distances, rather than the comparatively uncertain distance measurements that drive the uncertainty in individual speeds. For each pair,  $p_{ij}^2 \simeq \cos^2 \varphi$ , where  $\varphi$  is the angle between the comoving line-of-sight vector and the vector connecting the comoving supernova positions. This angle will be distributed randomly for each pair; the expected mean value of  $p_{ij}^2$  over a large number of pairs is 0.5. Thus the standard error in the mean pairwise velocity in a particular redshift and separation bin is

$$\delta v^{\text{est}}(r, a) = 2 \frac{\delta v_{\text{los}}(a)}{\sqrt{N(r, a)}}, \quad (30)$$

where  $N(r, a)$  is the total number of pairs used to estimate the mean pairwise velocity in a given redshift bin with mean scale factor  $a$  and separation bin with mean separation  $r$ .

The standard error on the projected statistic can be expressed as a sum over pairs in the same way as  $v(r, a)$ , except the sum is over  $N(\theta, z)$  pairs in a given angular separation bin about  $\theta$  instead of a given real-space separation  $r$ . The same calculation applies, except that now the average value of  $p_{ij}^2$  for a bin in  $\theta$  will not be 0.5. For a given pair, the projector  $p_{ij} = \pi_t / r$ , where  $\pi_t$  is the comoving radial separation of the pair (as defined in section III). Analogous to Eq. (29), the error on the projected statistic in a bin can be written as

$$\delta v^{\text{est}} = \sqrt{2} \delta v_{\text{los}} \left( \sum_{\text{pairs}} \frac{\pi_t^2}{r^2} \right)^{-1/2}. \quad (31)$$

The sum must be evaluated by integrating over all the pairs in a given angular bin, giving

$$\delta\tilde{v}(\theta, z) = \delta v_{\text{los}}(z) \left[ \frac{2}{N(\theta, z)} \int_0^{\pi_{\text{max}}} d\pi_t P(\pi_t|\theta, z) \frac{\pi_t^2}{\theta^2 d_C(z)^2 + \pi_t^2} \right]^{-1/2}, \quad (32)$$

with  $P(\pi_t|\theta, z)$  given by Eq. (15).

For a bin in angle covering a range from  $\theta_{\text{low}}$  to  $\theta_{\text{high}}$  and a mean redshift bin with a range from  $z_{\text{low}}$  to  $z_{\text{high}}$ , we can derive the number of pairs in this bin from Eq. (1). Consider a supernova at redshift  $z_1$ . Any second supernova which lies in the angular bin will be contained in a sky region with area  $2\pi(\cos\theta_{\text{low}} - \cos\theta_{\text{high}}) \simeq \pi(\theta_{\text{high}}^2 - \theta_{\text{low}}^2)$ , where the second expression is valid for small angles. The second supernova at redshift  $z_2 \geq z_1$  must satisfy  $z_{\text{low}} \leq (z_1 + z_2)/2 \leq z_{\text{high}}$  for the pair to be in the redshift bin, and  $c(z_2 - z_1)/H(z_1) < \pi_{\text{max}}$  for the comoving line-of-sight separation to be less than  $\pi_{\text{max}}$ . These conditions are equivalent to

$$z_{\text{low}} - \frac{\pi_{\text{max}} H(z_{\text{low}})}{2c} < z_1 < z_{\text{high}} \quad \text{and} \quad (33)$$

$$2z_{\text{low}} - z_1 < z_2 < \min \left[ 2z_{\text{high}} - z_1, z_1 + \frac{\pi_{\text{max}} H(z_1)}{c} \right]. \quad (34)$$

Then neglecting the effect of any spatial clustering of supernovae, the total number in the bin is simply

$$N(\theta_{\text{low}}, \theta_{\text{high}}; z_{\text{low}}, z_{\text{high}}) \simeq \pi(\theta_{\text{high}}^2 - \theta_{\text{low}}^2) \int dz_1 \frac{d^2 n}{dz d\Omega}(z_1) \int dz_2 \frac{d^2 n}{dz d\Omega}(z_2), \quad (35)$$

where the limits on the  $z$  integrals are given in Eqs. (33) and (34); note the  $z_2$  integral must be performed first since its limits depend on  $z_1$ . The function  $d^2 n/dz d\Omega$  is just Eq. (1) normalized to the total number of supernovae assumed per unit solid angle on the sky.

## B. Sample Variance

In addition to the measurement errors for individual galaxy velocities, there is an additional uncertainty in comparing estimates of the mean pairwise velocity to models, resulting from the fact that we only sample a finite volume in which the realized average pairwise velocity may differ from the mean taken over the entire Universe. Here we give an expression for the covariance between the projected mean pairwise velocity measured in different redshift and angular separation bins resulting from this effect (generally referred to as sample or cosmic variance).

Consider a mean pairwise velocity statistic binned in pair separation,  $r$ , and scale factor,  $a$ . For the three-dimensional mean pairwise velocity, Eq. (7), the sample covariance between two bins in separation and scale factor  $[r, a]_m$  and  $[r, a]_n$  for a survey volume  $V_\Omega$  can be written as [23]

$$C(r_m, r_n; a_m, a_n) = \frac{32\pi H(a_m) a_m H(a_n) a_n}{9V_\Omega (1 + \xi^{\text{gal}}(r_m, a_m))(1 + \xi^{\text{gal}}(r_n, a_n))} \times \left( \frac{d \ln D_a}{d \ln a} \right)_{a_m} \left( \frac{d \ln D_a}{d \ln a} \right)_{a_n} \int dk k^2 |P(k)|^2 j_1(kr_m) j_1(kr_n). \quad (36)$$

We now integrate along the line-of-sight accounting for the photo- $z$  errors and obtain an expression for the sample covariance of the projected mean pairwise velocity as a function of perpendicular separation,

$$C(\theta_m, \theta_n; a_m, a_n) = \int_0^\infty d\pi_{\text{obs}}^{(m)} \int_0^\infty d\pi_t^{(m)} P(\pi_t^{(m)}|\theta_m, a_m) P(\pi_{\text{obs}}^{(m)}|\pi_t^{(m)}) \times \int_0^\infty d\pi_{\text{obs}}^{(n)} \int_0^\infty d\pi_t^{(n)} P(\pi_t^{(n)}|\theta_n, a_n) P(\pi_{\text{obs}}^{(n)}|\pi_t^{(n)}) C(r_m, r_n; a_m, a_n), \quad (37)$$

using Eqs. (15) and (17).

The total statistical error covariance matrix is the sum of the sample covariance, Eq. (37), and the statistical error, Eq. (32):

$$C_{\text{total}}(\theta_m, \theta_n; a_m, a_n) = C(\theta_m, \theta_n; a_m, a_n) + \delta_{mn} \delta\tilde{v}^2(\theta_m, a_m). \quad (38)$$

In the following Section, we use this total covariance matrix to estimate the observability of SNeIa peculiar velocities and their utility to cosmology.

## VI. RESULTS

### A. The Signal-To-Noise Ratio of Projected Mean Pairwise Velocity Measurements

As seen in Fig. 1, the projected velocity statistic given by Eq. (12) is far less sensitive to photometric redshift errors than the non-projected pairwise velocity. We therefore will use this statistic both to estimate the signal-to-noise of pairwise velocity measurements and to determine the resulting constraints on cosmological parameters. The simple pairwise velocity should yield comparable or better constraints in the limit of small photometric redshift errors, but the results will be more sensitive to  $\sigma_z$ .

Figure 2 shows the signal-to-noise ratio per angular bin for measurements of the projected mean pairwise velocity as a function of angular separation  $\theta$ , for our fiducial survey giving  $3 \times 10^5$  total host galaxies over 300 square degrees of sky, and a distance modulus scatter for each host galaxy of  $\sigma_{SN} = 0.1$  plus the scatter due to lensing magnification. Pairs are binned in 6 redshift bins equally spaced between  $z = 0$  and  $z = 1.2$ . For each redshift bin, 10 bins in angle are used, equally spaced for angles ranging from  $\theta = 0$  up to the angle subtended by our maximum pair separation of 100 Mpc at the mean redshift for the redshift bin. The maximum angle considered therefore decreases as the redshift increases, causing the curves in Fig. 2 to truncate at differing values of  $\theta$ .

The mean pairwise velocity is detectable at a wide range of angular separations and redshifts. The top left panel of Figure 2 shows that such a measurement with a photometric redshift error of  $\sigma(z) = 0.01(1+z)$  yields a signal-to-noise ratio between 2 and 9 over a range in angular scales for all but the most extreme redshift bins with  $z > 0.8$ . The redshift distribution of observed SNeIa peaks around  $z = 0.5$  in our LSST-like model, so the closer we get to that redshift range, the more host galaxy pairs we average over and the better we can measure velocity statistics. Note also that although the number of pairs increases at larger separation, the amplitude of the mean pairwise velocity decreases, yielding an overall decrease in the signal-to-noise for bins with larger separations. The top right panel of Fig. 2 shows the signal-to-noise ratio for a photometric redshift error of  $\sigma_z = 0.02(1+z)$ . After this doubling of the photometric redshift error, the signal-to-noise decreases by around 30%. Even for  $\sigma_z = 0.03(1+z)$  (lower left panel of Fig. 2), we still reach a signal-to-noise of around 3 for the redshift bins at  $z = 0.5$  and  $z = 0.7$ .

The lower right panel shows a best-case scenario, assuming that spectroscopic redshifts are obtained for each supernova host galaxy; for simplicity, we define a spectroscopic redshift to have  $\sigma_z = 0.001(1+z)$ . This redshift error is generally obtainable only from spectroscopy of the hosts (rather than the SNe themselves), primarily because of the large breadth of SNIa spectral features, but also due to the peculiar velocities of SNe with respect to their galaxy’s center, which can reach a few hundred  $\text{km s}^{-1}$ . Spectroscopic redshifts for large samples of hosts (though likely not all, since many will be fainter than the SNe) would be quite feasible with a 5000-fiber, large field of view multi-object spectrograph like that currently proposed for the BigBOSS project [57]. If supernova samples cover 300 square degrees, as assumed above, a minimum of 43 BigBOSS pointings would be required to cover this sky region, yielding more than 200,000 redshifts; larger samples can be obtained by revisiting each pointing with different fiber placements. The proposed BigBOSS survey would use the Kitt Peak 4-meter telescope for only 100 nights per year; such a supernova project would require only a small fraction of the remaining time available. In this “spectroscopic limit,” the signal-to-noise in measuring the mean pairwise velocity generally improves by around a factor of two compared to the  $\sigma_z = 0.01(1+z)$  case.

### B. Parameter Space and Formalism

Now we investigate the constraints on dark energy parameters from a SNIa projected mean pairwise velocity measurement, and assess the complementarity of these constraints to performing the luminosity distance test based on the same data. For the sake of simplicity, we perform a Fisher matrix analysis similar to those in Refs. [17, 23]. In order to compute constraints on  $\Omega_\Lambda$ ,  $w_0$  and  $w_a$ , we marginalize over the remainder of the parameter space, consisting of the parameters  $\Delta_\zeta$ ,  $n_S$ , and  $h$ . We also treat  $\sigma_{z0}$ , describing the photometric redshift dispersion, as a parameter since the binned mean pairwise velocity signal depends on this quantity.

In addition to the marginalized constraints on  $\Omega_\Lambda$ ,  $w_0$ , and  $w_a$ , we quantify the additional constraining power of pairwise velocities by evaluating the quantity  $[\sigma(w_p)\sigma(w_a)]^{-1}$  for comparison to the DETF summary tables [43]. We refer to this as the “Figure of Merit” (FoM) for convenience, although in the DETF report this term refers to a slightly different quantity (the inverse area of the 95% confidence limit ellipse in the  $w_p - w_a$  plane) which is proportional to  $[\sigma(w_p)\sigma(w_a)]^{-1}$ . The derived parameter  $w_p$  is the equation of state at the “pivot” (i.e. best-constrained) redshift, defined as  $w_p = w_0 + (1 - a_p)w_a$  with  $a_p = 1 + [F^{-1}]_{w_0 w_a} / [F^{-1}]_{w_a w_a}$ .

The Fisher matrix for the projected mean pairwise velocity can be written as

$$F_{\alpha\beta} = \sum_{m,n} \frac{\partial \tilde{v}(m)}{\partial p_\alpha} C_{\text{total}}^{-1}(mn) \frac{\partial \tilde{v}(n)}{\partial p_\beta}, \quad (39)$$

where we have abbreviated the projected mean pairwise velocity in the  $n$ th angular separation and redshift bin as  $\tilde{v}(n)$ ,  $C_{\text{total}}(mn)$  is the total covariance matrix between bins  $m$  and  $n$  given by Eq. (38), and  $p_\alpha$  indexes the parameters in the vector  $\mathbf{p}$ . The Fisher matrix provides a local estimate of the parameter covariance, so the standard error on parameter  $p_\alpha$  marginalized over the other parameters is  $\sigma(p_\alpha) = [F^{-1}]_{\alpha\alpha}$  (no summation implied).

Prior constraints on any of the parameters  $\mathbf{p}$  which are normally distributed are simple to incorporate. If parameter  $p_\alpha$  has a Gaussian prior with standard error  $\sigma_\alpha$ , we simply add the diagonal matrix  $\text{diag}(1/\sigma_\alpha^2)$  to the Fisher matrix  $F_{\alpha\beta}$ . Priors with non-normal statistical distributions require a more detailed statistical framework rather than a simple Fisher matrix approximation.

### C. Statistical Constraints on Dark Energy Parameters

In computing constraints on the dark energy parameters  $\Omega_\Lambda$ ,  $w_0$ , and  $w_a$ , we first assume a reasonable calibration spectroscopic sample of 1500 SNeIa, comprising 250 supernovae in each redshift bin spread uniformly over the 6 redshift bins spanning  $0 < z < 1.2$ . The fractional error on the photo- $z$  dispersion,  $\delta\sigma_{z0}/\sigma_{z0}$  in this case is around  $1/\sqrt{500}$ , or approximately 5% (assuming Gaussian errors). We therefore incorporate a Gaussian prior on  $\sigma_{z0}$  centered on the true value and with  $\sigma = 0.05\sigma_{z0}$ ; however, as we show below in Fig. 4, the pairwise velocity statistic is relatively insensitive to the choice of a prior on  $\sigma_{z0}$ , so this choice should not significantly affect our results, even if the actual error on  $\sigma_{z0}$  is much larger.

We compute the standard errors obtainable on the dark energy parameters using a range of supernova distance modulus dispersions  $\sigma_{\text{SN}}$  and photometric redshift dispersions  $\sigma_{z0}$ . We consider three possible values of the intrinsic supernova absolute magnitude dispersion given by  $\sigma_{\text{SN}} = 0.05$ ,  $\sigma_{\text{SN}} = 0.1$ , and  $\sigma_{\text{SN}} = 0.2$ . For each value of  $\sigma_{\text{SN}}$ , we explore four possible values of photometric redshift dispersion,  $\sigma_{z0} = 0.001$  (the ‘‘spectroscopic limit’’),  $\sigma_{z0} = 0.01$ ,  $\sigma_{z0} = 0.02$ , and  $\sigma_{z0} = 0.03$ . The optimistic but reasonable supernova luminosity distance test assumed in the DETF report corresponds to  $\sigma_{\text{SN}} = 0.1$  and  $\sigma_{z0} = 0.01$  so these choices constitute a sensible baseline for comparison to other techniques.

The strength of the dark energy constraints obtained is relatively sensitive to the amount of prior information assumed. First, we can make the same assumptions used by the Dark Energy Task Force [43]. They assume constraints on all parameters (including covariances) at the level expected for measurements of the microwave background power spectrum by the Planck satellite. For this, we employ the Planck Fisher Matrix provided by the DETF. In addition, DETF assume a 11% Gaussian prior on the value of  $h$  [58]. Note that a spatially flat universe is *not* assumed. We also assume no systematic error on either redshift or distance modulus measurements; limits on these systematics required to attain the statistical error levels presented here are discussed below. The results are given in Table I.

For the nominal DETF survey case, mean pairwise velocities give a standard error on  $w_0$  of  $\sigma(w_0) = 0.45$  and a standard error on  $w_a$  of  $\sigma(w_a) = 0.98$ . This constraint on  $w_0$  is comparable to the DETF Stage-IV constraints from ground-based optical baryon acoustic oscillations or galaxy cluster counts, while not as good as those from Stage-IV supernova luminosity distances. For  $w_a$ , mean pairwise velocity constraints are significantly better than the optical survey-based BAO projection; slightly weaker than the pessimistic BAO projections for space-based or radio observations and for the optimistic galaxy cluster projection; and halfway between the optimistic and pessimistic DETF supernova luminosity distance projection. However, all of these methods trail the Stage IV weak lensing projections in constraining power.

Among the dark energy probes resulting from a large ground-based optical survey like LSST, mean pairwise velocities compare well with both the baryon acoustic oscillation and the supernova luminosity distance probes [17]. To quantify this, we consider the improvement in dark energy parameters obtained by adding the mean pairwise velocity probe to the supernova luminosity distance probe resulting from the same sample. The mean pairwise velocity can be measured using the supernova data from a large survey telescope with little additional cost compared to simply constraining dark energy using the resulting supernova Hubble diagram.

Figure 3 shows joint constraints on the dark energy parameters combining projected peculiar velocity measurements and the SNIa luminosity distance test, using the same priors as Table I. The left panel shows the  $1\sigma$  constraint in the  $w_0 - \Omega_\Lambda$  plane and the right panel shows the constraint in the  $w_a - \Omega_\Lambda$  plane, after marginalizing over the remainder of parameter space. Incorporating peculiar velocity information significantly reduces the size of the ellipses in the dark energy parameter space: the marginalized constraint on  $\Omega_\Lambda$  improves by a factor of 1.7, on  $w_0$  by a factor of 1.2, and on  $w_a$  by a factor of 1.5, giving an overall improvement in the Figure of Merit by a factor of 1.8. (As a

	$\sigma_{z0} = 0.001$			$\sigma_{z0} = 0.01$			$\sigma_{z0} = 0.02$			$\sigma_{z0} = 0.03$		
$\sigma_{\text{SN}}$	$\sigma(\Omega_\Lambda)$	$\sigma(w_0)$	$\sigma(w_a)$	$\sigma(\Omega_\Lambda)$	$\sigma(w_0)$	$\sigma(w_a)$	$\sigma(\Omega_\Lambda)$	$\sigma(w_0)$	$\sigma(w_a)$	$\sigma(\Omega_\Lambda)$	$\sigma(w_0)$	$\sigma(w_a)$
0.05	0.016	0.22	0.36	0.032	0.28	0.48	0.05	0.43	0.89	0.059	0.78	1.7
0.1	0.039	0.30	0.55	0.056	0.45	0.98	0.094	0.62	2.52	0.13	1.46	2.81
0.2	0.051	0.42	0.72	0.074	0.59	1.84	0.18	1.36	4.71	0.24	2.87	6.14

TABLE I: Dark energy parameter constraints derived from mean pairwise velocity statistics. Photometric redshifts are assumed to be normally distributed about the true  $z$ , with  $\sigma_z = \sigma_{z0}(1+z)$ . We show results for  $\sigma_{z0} = 0.001, 0.01, 0.02$ , and  $0.03$ , and three different values for the uncertainty in supernova distance moduli,  $\sigma_{\text{SN}} = 0.05, 0.1$  and  $0.2$ . The fiducial values of the dark energy parameters are  $\Omega_\Lambda = 0.75$ ,  $w_0 = -1$  and  $w_a = 0$ . We assume zero systematic errors related to SNIa evolution, i.e.  $\mu_L = \mu_Q = 0$ . We assume the same priors used in the DETF report: Planck satellite priors from its projected measurement of the microwave background power spectrum (using the Fisher matrix supplied by the DETF) and a Gaussian prior on  $h$  with a standard error of 11%. This table does not assume a flat spatial geometry for the universe.

point of comparison, corresponding constraints with no priors from other measurements are included in Fig. 4.) Note that unlike the case of peculiar velocity measurements, the constraints derived from the SNIa luminosity distance are sensitive to the error in mean redshift of a bin and hence the cosmological constraints derivable from the SNIa luminosity distance depend much more on the amount of prior knowledge of the photo- $z$  distribution [17, 59], as well as being much more sensitive to intrinsic SNIa luminosity evolution.

We have also considered statistical dark energy constraints from a more constraining, but still realistic, set of priors. In particular, a measurement of the Hubble parameter based on an improved, NGC 4258-calibrated distance ladder with an estimated overall error of 5% has recently been reported [60]. Furthermore, requiring the dark energy probe itself in combination with microwave background data to determine the geometry of the universe is likely overly restrictive. Measurements of the baryon acoustic oscillation scale from the Sloan Digital Sky Survey Data Release 7, combined with WMAP 5-year data, give a constraint on the curvature parameter of  $\Omega_k = -0.013 \pm 0.007$ , even for a very general cosmological model which allows both a nonflat universe and a value of  $w_0$  different from -1 [61]. Additionally, since a flat universe is an unstable fixed point for standard cosmological evolution, we have an overwhelming theoretical prejudice for  $\Omega_k = 0$  to high precision. Therefore, a prior assumption of a flat universe is both reasonable and strongly suggested by data.

Table II gives the standard errors on the dark energy parameters for a flat universe, with gaussian priors for  $h$  (5%),  $\Delta_\zeta$  (5%), and  $n_S$  (1%), the latter two being current limits from WMAP 7-year data [62]. The assumption of a flat universe and a tighter prior on  $h$  lead to much stronger dark energy constraints than do DETF priors. With these priors, a DETF-assumed supernova sample with  $\sigma_{\text{SN}} = 0.1$  and  $\sigma_{z0} = 0.01$  gives a measurement of  $\Omega_\Lambda$ ,  $w_0$  and  $w_a$  with standard errors of 0.024, 0.27, and 0.41, respectively, using the mean pairwise velocity alone. For comparison, the constraints on  $w_0$  for Stage IV experiments computed in the DETF report (but for the original set of priors) are worse for clusters, comparable for baryon acoustic oscillations, and better for the supernova Hubble diagram. Our constraint on  $w_a$ , on the other hand, is better than for any of the Stage IV experiments aside from the optimistic weak lensing scenarios.

Of course, the constraining power of other probes will also increase with the more restrictive set of priors we assume in Table II. This makes a direct comparison with these other methods beyond the scope of this paper. Our primary point is that under optimistic, but reasonable, assumptions, SNIa peculiar velocities can be useful by themselves and at the very least can serve as a valuable complementary probe and cross-check for systematic errors, while requiring little additional investment. However, note that Table II shows that broader photo- $z$  distributions and/or larger intrinsic SNIa dispersions can quickly diminish the returns on SNIa peculiar velocities.

This calculation also suggests the potential constraining power of pairwise velocity statistics from future survey observations. If a large photometric supernova survey were combined with follow-up spectroscopic redshifts for supernova host galaxies, the standard error in the redshift could be reduced by a factor of 10 to  $\sigma_{z0} = 0.001$ , corresponding to the first column of Table II. In this case, the error on  $w_0$  shrinks to  $\sigma(w_0) \simeq 0.10$  and the error on  $w_a$  is nearly  $\sigma(w_a) \simeq 0.16$ . Understanding Type-Ia supernovae well enough to push  $\sigma_{\text{SN}}$  down by a factor of 2 to  $\sigma_{\text{SN}} = 0.05$  would reduce the error on  $w_a$  by another factor of two, to 0.08. Few other proposed probes have comparable potential to constrain  $w_a$ .

	$\sigma_{z0} = 0.001$			$\sigma_{z0} = 0.01$			$\sigma_{z0} = 0.02$			$\sigma_{z0} = 0.03$		
$\sigma_{\text{SN}}$	$\sigma(\Omega_\Lambda)$	$\sigma(w_0)$	$\sigma(w_a)$	$\sigma(\Omega_\Lambda)$	$\sigma(w_0)$	$\sigma(w_a)$	$\sigma(\Omega_\Lambda)$	$\sigma(w_0)$	$\sigma(w_a)$	$\sigma(\Omega_\Lambda)$	$\sigma(w_0)$	$\sigma(w_a)$
0.05	0.004	0.047	0.08	0.012	0.16	0.23	0.024	0.34	0.49	0.049	0.65	1.03
0.1	0.009	0.10	0.16	0.024	0.27	0.41	0.046	0.62	0.94	0.1	1.42	1.96
0.2	0.022	0.28	0.41	0.061	0.63	0.89	0.1	1.48	1.93	0.2	2.86	4.18

TABLE II: Same as Table I, but we assume  $\Omega_k = 0$  and instead of Planck priors we assume Gaussian priors with standard errors of 5% on  $h$  and  $\Delta_\zeta$  and 1% on  $n_s$  (comparable to errors from current measurements).

$\mu_L = \mu_Q$	$\Omega_\Lambda$	$w_0$	$w_a$
$0.01/\sqrt{2}$	10.2%	4.1%	20.2%
$0.03/\sqrt{2}$	20.3%	10.0%	41.0%
$0.05/\sqrt{2}$	40.9%	37.5%	80.1%

TABLE III: The ratio of the parameter bias due to systematic error to the statistical uncertainties on these parameters. A photometric redshift distribution with dispersion  $\sigma_z = 0.01(1+z)$  is assumed. We assume  $\mu_L = \mu_Q$  to compute the systematic bias. Then we set  $\mu_L = \mu_Q = 0$  and compute the statistical uncertainty and report the ratio of systematic bias to statistical errors  $\Delta p/\sigma_p$ , where  $p = \Omega_\Lambda, w_0, \text{ or } w_a$ . We assume  $\Omega_k = 0$  and assume Gaussian priors with standard error of 5% on  $h$  and  $\Delta_\zeta$  and 1% on  $n_s$ .

#### D. Systematic Error in Distance Modulus

The potential statistical sensitivity of any dark energy probe can only be realized if systematic errors can be controlled to a level where their effect on cosmological parameters is small compared to the statistical errors. For the supernova data set considered here, systematic errors may effect both observables: the distance modulus and the photometric redshift. This section considers distance modulus systematics, while the following section analyzes the effect of redshift errors.

Section IV B gives a simple phenomenological model for the effect of SNIa evolution with redshift, in terms of the parameters  $\mu_L$  and  $\mu_Q$ . The resulting systematic error on cosmological parameters induced by this systematic error can be estimated using a Fisher matrix approach. The bias in parameter  $p_\alpha$  can be written as

$$\delta p_\alpha = \sum_\beta [F^{-1}]_{\alpha\beta} \sum_{m,n} \Delta \tilde{v}(m) C_{\text{total}}^{-1}(mn) \frac{\partial \tilde{v}(n)}{\partial p_\beta} \quad (40)$$

where  $\Delta \tilde{v}$ , obtained by substituting Eq. (24) for  $v(r, a)$  in Eq. (12), is the systematic shift in the observable  $\tilde{v}$  due to the systematic error characterized by nonzero values of  $\mu_L$  and  $\mu_Q$ .

We calculate the bias in each parameter due to SNIa evolution assuming a photometric redshift distribution with spread  $\sigma_z = 0.01(1+z)$  and the evolution model given by Eq. (19). We can then compare the systematic bias with the statistical errors on dark energy parameters assuming  $\mu_L = \mu_Q = 0$ , as computed in Table II. The ratios of the bias of the dark energy parameters to their statistical errors are reported in Table III for several representative choices of  $\mu_L$  and  $\mu_Q$ . For reference, DETF took evolution in SNIa luminosity with  $\mu_L = \mu_Q = 0.01/\sqrt{2}$  as their optimistic scenario. We find that the maximum bias incurred in  $\Omega_\Lambda$  and  $w_0$  is less than 40% as large as the statistical error on these parameters as long as  $\mu_L = \mu_Q \leq 0.05/\sqrt{2}$  (five times larger than the DETF optimistic systematic error). For  $w_a$ , the systematic bias is 40% of the statistical error for  $\mu_L = \mu_Q \leq 0.03/\sqrt{2}$ , and increases to 80% of the statistical error for  $\mu_L = \mu_Q = 0.05/\sqrt{2}$ . If the actual unrecognized evolution of SNIa luminosity is similar to that assumed in the DETF report, the resulting systematic bias in dark energy parameters should be insignificant compared to the statistical error. Note that these comparisons conservatively use the statistical error incorporating our more restrictive prior than in the DETF report. The larger statistical errors with the DETF priors admit substantially larger systematic errors.

#### E. Systematic Errors in Photometric Redshifts

We have also tested how a possible bias  $\Delta z_p$  in the photo- $z$  distribution might impact the dark energy constraints obtainable from pairwise velocity statistics. If  $\Delta z_p$  is not a strong function of redshift (i.e., it does not vary considerably

$\sigma(\sigma_{z0})$	$\sigma(\Omega_\Lambda)$	$\sigma(w_0)$	$\sigma(w_a)$
no prior	0.046	0.29	0.62
prior (100% error in $\sigma_{z0}$ )	0.023	0.25	0.37
prior (zero error in $\sigma_{z0}$ )	0.018	0.21	0.31

TABLE IV: Impact of prior information about photo-z distributions on the dark energy parameter constraints derived from mean pairwise velocity statistics (calculated in the absence of complementary cosmological probes). The photometric redshift of an SN is assumed to be normally distributed about its true value with  $\sigma_z = \sigma_{z0}(1+z)$ ; for our standard scenario we take  $\sigma_{z0} = 0.01$ . The fiducial values cosmology considered has  $\Omega_\Lambda = 0.75$ ,  $w_0 = -1$  and  $w_a = 0$ . We assume  $\Omega_k = 0$  and assume Gaussian priors with standard error of 5% on  $h$  and  $\Delta_c$  and 1% on  $n_s$ .

within one of our redshift bins with width  $\delta z \simeq 0.2$ ), then the bias affects both galaxies in each pair in approximately the same manner. The mean pairwise velocity relies on the difference between the two velocities so nearly all of the effects of a photo-z bias tend to cancel. The residual is a small misestimation of the location of the redshift bin, which translates into a small error in cosmological parameters. For example, assuming a bias in photometric redshifts of  $\Delta z_p \approx 0.002(1+z)$  degrades the constraints on cosmological parameters by less than 2% of the statistical errors. This stands in stark contrast to the strong dependence of the luminosity distance test on photometric redshift biases (e.g., [17, 59]) and the similar sensitivity of probes such as weak gravitational lensing to biased photometric redshifts (e.g., [63]).

The signal we measure, the redshift-binned projected mean pairwise velocity Eq. (18), depends on the scatter in photometric redshifts so we also must estimate the systematic error due to uncertainty in the photometric redshift dispersion. We assume that the distribution of the difference between photo-z's and spectroscopic redshifts is a standard normal distribution; in reality this distribution is likely more complex. The results here are a simple effective model for the distribution of photometric redshifts.

Figure 4 and Table IV show marginalized statistical constraints on dark energy parameters from mean pairwise velocity only, under three strongly different assumptions regarding the photometric redshift error. The blue (gray) and the black shaded regions show the two extreme cases. The blue shaded area shows the  $1\sigma$  constraint when we assume no prior knowledge of the uncertainty in the photo-z error and allow  $\sigma_{z0}$  to be determined from the same data used to constrain cosmology. The black region indicates the constraints when  $\sigma_{z0}$  is known exactly. We emphasize that this does not mean that the photometric redshift is equal to the true redshift. There is still a non-negligible dispersion in photometric redshifts in this case; however, we have assumed that the photometric redshift distribution is well understood, perhaps due to calibration with several thousand spectra [17]. The red (light shaded) region represents the case when the prior on  $\sigma_{z0}$  is a Gaussian centered at the true value with sigma equal to its fiducial value,  $\sigma_{z0} = 0.01$ .

Constraints on  $w_0$ ,  $w_a$  and  $\Omega_\Lambda$  change by only about 10% between the case where  $\sigma_{z0}$  is uncertain at the 100% level and one where we assume a perfectly-calibrated photometric redshift distribution. This results from the fact that the mean pairwise velocity is proportional to the redshift difference between galaxies in a pair, but photometric redshift errors do not correlate with the velocity we are trying to measure. Fig. 4 shows that even weak prior knowledge of the photo-z distribution yields constraints comparable to a scenario where the photo-z error distribution is known exactly.

## VII. DISCUSSION AND FUTURE PROSPECTS

With vastly increased numbers of Type Ia supernova detections on the horizon, a new statistical probe of dark energy using supernova peculiar velocities will be possible. The Dark Energy Task Force, when considering future supernova measurements, made the optimistic but reasonable assumptions that individual supernovae will have a photometric redshift determined with a standard error 0.01 at redshift  $z = 0$ , and a distance modulus determined with an error of 0.1. If these levels are attained for the nominal  $3 \times 10^5$  SNeIa which will be detected in a targeted supernova survey area by the LSST, the resulting dark energy constraints from the mean pairwise velocities of these supernovae are interestingly good, comparable to projections for a variety of Stage IV techniques. In particular, pairwise peculiar velocities alone give a slightly stronger dark energy constraint as the optimistic projection for an optical baryon acoustic oscillation probe, and constraints which are towards the optimistic ends of the galaxy cluster abundance and optical supernova Hubble diagram probes.

Having another independent method for constraining dark energy is invaluable, since all of these measurements will likely be limited by systematic error control. Comparison of inferred dark energy parameters from multiple

independent experiments is even more important than the combined statistical power of multiple measurements. In addition, the science return from mean pairwise velocity measurements comes essentially “for free,” as it uses the same data sets from which supernova luminosity distance measurements will be built.

An extension of these observations which can significantly improve the strength of dark energy constraints is the addition of spectroscopic redshifts. Surveys like Pan-STARRS and LSST will provide only photometric redshifts, and the sheer number of objects they observe makes obtaining spectroscopic redshifts for even small subsets of the total objects a massive challenge. Given the numbers used in this paper, LSST will detect on the order of 100 new SNeIa per night of the survey. The supernovae themselves are transient and widely spread over the survey area, limiting the total number which can be observed simultaneously. Obtaining immediate redshift follow-up for all of these objects would be a large logistical challenge, even if a dedicated telescope were available. An alternative is to obtain redshifts of host galaxies after their SNe have faded; this can be done much more efficiently, as many host galaxies in a particular field of view could be targeted simultaneously with multi-object spectrographs. Baryon acoustic oscillation observations, in particular, are pioneering the development of very large fiber spectrographs which can obtain thousands of redshifts simultaneously. The challenge for this strategy is that many of the host galaxies will be at redshifts above 0.5, and many of the host galaxies themselves are dim compared to their supernovae. Host galaxy followup would require a large telescope and large amounts of observing time. The spectrograph proposed for the BigBOSS survey, which has been designed to obtain high-throughput spectroscopy of 5000 galaxies at a time over a 7 square degree field of view using the 4m Mayall telescope at Kitt Peak and the Blanco telescope at CTIO [57], would be well suited for this task. Such a spectroscopic survey of supernova hosts would be a major undertaking, but could lead to highly competitive dark energy constraints and leverages instruments and data already planned for other purposes.

Another possible avenue for improvement is better standardization of SNIa intrinsic luminosities. Here our baseline assumption, along with the DETF, is that SNIa distance moduli will be known with a standard error of around 0.1. It is an open question whether we eventually will understand the SNIa explosion mechanism in enough detail, and have sufficient observational information, to model some portion of this scatter and reduce the effective random error. Magnification due to gravitational lensing provides an additional source of scatter, which can be partly understood due to its strongly non-Gaussian distribution, but for our nominal model survey we are not limited by lensing scatter. The marginalized constraint on  $w_a$ , the most challenging dark energy parameter to measure, can be improved by a factor of two if the scatter in the intrinsic supernova distance modulus is halved. A mean pairwise velocity measurement for  $3 \times 10^5$  supernovae with spectroscopic redshifts and an intrinsic distance modulus scatter of 0.05 would constrain  $w_a$  with a standard error of 0.08 using our set of current prior constraints.

The statistical power of any given dark energy measurement is only half of the story, as all of these measurements are likely to be heavily dependent on systematic error control. Because of its nature as a differential measurement, the mean pairwise velocity technique offers favorable prospects for controlling systematic errors. Differential measurements have long been exploited in measurements of the cosmic microwave background fluctuations precisely for their systematic error advantages. In particular, we have demonstrated that several obvious systematic error sources are not likely to dominate the dark energy constraints. First, uncertainty about the level of scatter in photometric redshifts about their true values has only a weak effect on dark energy constraints, and mild priors obtainable from modest spectroscopic calibration efforts give results that are nearly the same as exact knowledge of the photometric redshift scatter. We have not considered non-Gaussian errors in photometric redshifts, but any scatter which is characterized at the levels of the normal errors considered here is unlikely to induce any significantly larger systematic errors.

Second, a bias in the photometric redshift distribution has very little effect on our constraints, as long as the bias varies slowly with redshift, because a constant redshift bias doesn’t affect the pairwise velocities. This is in marked contrast to both the supernova luminosity distance and weak lensing techniques. Both of these widely discussed routes to dark energy constraints are very sensitive to photometric redshift biases [17, 59], where a redshift bias can mimic a shift in dark energy parameters. Third, a systematic error in distance modulus due to unrecognized evolution in mean supernova luminosity with redshift will be a small effect provided the magnitude of the error is within a factor of 3 of that considered in the DETF report. This potential source of error can also be addressed by testing the rich information in supernova spectra and time series at different redshifts for any evidence of evolution in intrinsic supernova properties. While detailed modeling of potential systematic errors is required to understand any particular experiment, it is plausible that the systematic errors associated with mean pairwise velocities will be substantially less severe than other leading techniques for probing dark energy.

We also note that mean pairwise velocities can be used to constrain gravitational explanations for the accelerating expansion of the universe. This technique has the advantage of probing structure growth over a wide range in redshift, while also being sensitive to the expansion rate; the comparison between these two quantities is the key to constraining alternate gravity models [64–66]. Pairwise velocities from a much smaller sample of galaxy clusters, with more precise velocities obtained via the kinematic Sunyaev-Zeldovich effect, have already been shown to offer potentially interesting constraints on modifications of gravity [14].

The pairwise velocity statistic offers a particularly simple route to a probe of modified gravity. In linear perturbation



theory, the evolution of the growth factor  $D(a)$  is given to a very good approximation by  $d \ln D / d \ln a = \Omega(a)^\gamma$ , where  $\gamma$  is nearly a constant and takes the value  $\gamma \approx 0.55$  for general relativity [4]; see Ref. Juskiewicz et al. [67] for a highly accurate approximation to  $D(a)$ . Other gravitation theories can have different values of  $\gamma$ ; for example, DGP gravity [68] has  $\gamma = 0.68$  [8]. Examining Eq. (7), we see that the mean pairwise velocity (on the left side) depends linearly on  $d \ln D / d \ln a$ , as well as  $H(a)$ , the (linear regime) galaxy bias factor, and correlation function information. Other cosmological tests, such as the supernova Hubble diagram, will directly constrain  $H(a)$ , while correlation functions will be measurable directly from the data set used. The linear clustering bias of host galaxies can be constrained in a number of ways; e.g., by direct comparison of galaxy correlation functions to the matter power spectrum derived from gravitational lensing; with galaxy three-point correlation functions [69] or angular bispectra [70]; or (if a large spectroscopic sample is available) by combining redshift-space distortions [19–21] with mean pairwise velocity statistics. Assuming these other quantities will be measured with errors which are small compared to our velocity errors, a measurement of  $v(r, a)$  will provide an estimate of  $d \ln D / d \ln a$  in several bins in  $a$ , which can then be used to constrain  $\gamma$ .

If for each bin in  $a$  we have independent measurements of  $v(r, a)$  in five radial bins with a signal-to-noise ratio of around 3 in each bin (see Fig. 2), then the amplitude of the function  $v(r, a)$  can be constrained with a fractional error of around  $0.33/\sqrt{5}$  or 0.16. Assuming this is the dominant error, the fractional error on  $d \ln D / d \ln a$  is also around 0.16. By propagation of errors, the resulting error on  $\gamma$  is then  $0.16 / \ln \Omega_m(a)$ , and hence ranges from 0.15 to 0.45, depending on the redshift bin. This would give approximately a 25% to 80% measurement of  $\gamma$  in each redshift bin (assuming  $\gamma$  takes its general relativistic value), providing a significant constraint on many theoretical alternatives to general relativity. With spectroscopic redshifts, these constraints would improve by a factor of three due to the increase in signal-noise ratio in each angular bin; then the best redshift bin alone might provide a 10% measurement of  $\gamma$ , comparable to projected constraints from weak lensing [12]. Prospects for constraining modified gravity with a large supernova survey will be explored in more detail elsewhere.

Dark energy is simultaneously one of the most important problems in physics today, and one of the most elusive to address observationally. Mean pairwise velocities extracted from a large survey of SNeIa can provide an important arrow in the dark energy quiver and should be considered alongside any of the other methods now being actively pursued. If simply piggybacked on existing plans for supernova luminosity distance tests, pairwise velocities offer independent dark energy constraints which are competitive with other methods. If augmented by spectroscopic redshift followup observations, pairwise velocities alone may provide important constraints on dark energy, with constraints on  $w_a$  of 0.1 or better. Perhaps most importantly, this technique provides not only statistical power but potentially strong control of systematic errors. Additionally, it allows tests of the nature of gravity which cannot be obtained using distance measurements alone. We anticipate that Type Ia supernova peculiar velocity statistics will be in the vanguard of dark energy constraints over the coming years.

### Acknowledgments

The authors would like to thank Michael Wood-Vasey for useful discussions about the potential of imaging surveys to improve cosmological constraints from Type Ia supernovae and Daniel Holz for discussion about the lensing of supernovae. An anonymous referee provided a number of helpful suggestions to clarify various points, and prompted discovery of a factor-of-two mistake in computing statistical errors. SB was partly supported by the Mellon Predoctoral Fellowship at the University of Pittsburgh during this project and the LDRD program of Los Alamos National Lab. ARZ is funded by the University of Pittsburgh, the National Science Foundation through grant AST 0806367, and by the Department of Energy. AK is supported by NSF grant AST 0807790. JAN is funded by the University of Pittsburgh, the National Science Foundation through grant AST 0806732, and by the Department of Energy.

- 
- [1] A. G. Riess, A. V. Filippenko, P. Challis, A. Clocchiatti, A. Diercks, P. M. Garnavich, R. L. Gilliland, C. J. Hogan, S. Jha, R. P. Kirshner, et al., *AJ* **116**, 1009 (1998), arXiv:astro-ph/9805201.
  - [2] S. Perlmutter, G. Aldering, G. Goldhaber, R. A. Knop, P. Nugent, P. G. Castro, S. Deustua, S. Fabbro, A. Goobar, D. E. Groom, et al., *ApJ* **517**, 565 (1999), arXiv:astro-ph/9812133.
  - [3] J. Zhang, L. Hui, and A. Stebbins, *ApJ* **635**, 806 (2005), astro-ph/0312348.
  - [4] E. V. Linder, *Phys. Rev. D* **72**, 043529 (2005), arXiv:astro-ph/0507263.
  - [5] H. Zhan and L. Knox, *ArXiv Astrophysics e-prints* (2006), arXiv:astro-ph/0611159.
  - [6] Y. Wang, G. Narayan, and M. Wood-Vasey, *MNRAS* **382**, 377 (2007), 0708.0033.
  - [7] D. Huterer and E. V. Linder, *Phys. Rev. D* **75**, 023519 (2007), arXiv:astro-ph/0608681.
  - [8] E. V. Linder and R. N. Cahn, *Astroparticle Physics* **28**, 481 (2007), arXiv:astro-ph/0701317.

- [9] H. Zhan, L. Knox, and J. A. Tyson, ArXiv e-prints (2008), 0806.0937.
- [10] M. J. Mortonson, W. Hu, and D. Huterer, ArXiv e-prints (2008), 0810.1744.
- [11] P. Zhang and X. Chen, Phys. Rev. D **78**, 023006 (2008), 0710.1486.
- [12] A. P. Hearin and A. R. Zentner, JCAP **4**, 32 (2009), 0904.3334.
- [13] G. Zhao, T. Giannantonio, L. Pogosian, A. Silvestri, D. J. Bacon, K. Koyama, R. C. Nichol, and Y. Song, arXiv:1003.0001 (2010), 1003.0001.
- [14] A. Kosowsky and S. Bhattacharya, Phys. Rev. D **80**, 062003 (2009), 0907.4202.
- [15] R. B. Metcalf, MNRAS **305**, 746 (1999).
- [16] S. Dodelson and A. Vallinotto, Phys. Rev. D **74**, 063515 (2006), arXiv:astro-ph/0511086.
- [17] A. R. Zentner and S. Bhattacharya, ApJ **693**, 1543 (2009), 0812.0358.
- [18] F. Schmidt, Phys. Rev. D **78**, 043002 (2008), 0805.4812.
- [19] E. V. Linder, Astroparticle Physics **29**, 336 (2008), 0709.1113.
- [20] M. White, Y.-S. Song, and W. J. Percival, ArXiv e-prints (2008), 0810.1518.
- [21] W. J. Percival and M. White, ArXiv e-prints (2008), 0808.0003.
- [22] S. Bhattacharya and A. Kosowsky, ApJ **659**, L83 (2007), arXiv:astro-ph/0612555.
- [23] S. Bhattacharya and A. Kosowsky, Phys. Rev. D **77**, 083004 (2008), 0712.0034.
- [24] S. Bhattacharya and A. Kosowsky, JCAP **8**, 30 (2008), 0804.2494.
- [25] T. Haugbølle, S. Hannestad, B. Thomsen, J. Fynbo, J. Sollerman, and S. Jha, ApJ **661**, 650 (2007), arXiv:astro-ph/0612137.
- [26] P. G. Ferreira, R. Juszkiewicz, H. A. Feldman, M. Davis, and A. H. Jaffe, ApJ **515**, L1 (1999), arXiv:astro-ph/9812456.
- [27] R. K. Sheth, L. Hui, A. Diaferio, and R. Scoccimarro, MNRAS **325**, 1288 (2001), arXiv:astro-ph/0009167.
- [28] H. Feldman, R. Juszkiewicz, P. Ferreira, M. Davis, E. Gaztañaga, J. Fry, A. Jaffe, S. Chambers, L. da Costa, M. Bernardi, et al., ApJ **596**, L131 (2003), arXiv:astro-ph/0305078.
- [29] D. Sarkar, H. A. Feldman, and R. Watkins, MNRAS **375**, 691 (2007), arXiv:astro-ph/0607426.
- [30] S. Courteau, J. A. Willick, M. A. Strauss, D. Schlegel, and M. Postman, ApJ **544**, 636 (2000), arXiv:astro-ph/0002420.
- [31] S. Borgani, M. Bernardi, L. N. da Costa, G. Wegner, M. V. Alonso, C. N. A. Willmer, P. S. Pellegrini, and M. A. G. Maia, ApJ **537**, L1 (2000), arXiv:astro-ph/0005450.
- [32] S. Borgani, L. N. da Costa, I. Zehavi, R. Giovanelli, M. P. Haynes, W. Freudling, G. Wegner, and J. J. Salzer, AJ **119**, 102 (2000), arXiv:astro-ph/9908155.
- [33] J. P. Blakeslee, M. Davis, J. L. Tonry, E. A. Ajhar, and A. Dressler, in *Cosmic Flows Workshop*, edited by S. Courteau & J. Willick (2000), vol. 201 of *Astronomical Society of the Pacific Conference Series*, pp. 254–+.
- [34] R. Watkins and H. A. Feldman, MNRAS **379**, 343 (2007), arXiv:astro-ph/0702751.
- [35] H. A. Feldman and R. Watkins, MNRAS **387**, 825 (2008), 0802.2961.
- [36] H. A. Feldman, R. Watkins, and M. J. Hudson, ArXiv e-prints (2009), 0911.5516.
- [37] A. Dekel, A. Eldar, T. Kolatt, A. Yahil, J. A. Willick, S. M. Faber, S. Courteau, and D. Burstein, ApJ **522**, 1 (1999), arXiv:astro-ph/9812197.
- [38] J. D. Neill, M. J. Hudson, and A. Conley, ApJ **661**, L123 (2007), 0704.1654.
- [39] L. Hui and P. B. Greene, Phys. Rev. D **73**, 123526 (2006), arXiv:astro-ph/0512159.
- [40] A. Cooray and R. R. Caldwell, Phys. Rev. D **73**, 103002 (2006), arXiv:astro-ph/0601377.
- [41] A. Abate and O. Lahav, MNRAS **389**, L47 (2008), 0805.3160.
- [42] C. Gordon, K. Land, and A. Slosar, Phys. Rev. Lett. **99**, 081301 (2007), 0705.1718.
- [43] A. Albrecht, G. Bernstein, R. Cahn, W. L. Freedman, J. Hewitt, W. Hu, J. Huth, M. Kamionkowski, E. W. Kolb, L. Knox, et al., ArXiv Astrophysics e-prints (2006), astro-ph/0609591.
- [44] E. Komatsu, J. Dunkley, M. R.olta, C. L. Bennett, B. Gold, G. Hinshaw, N. Jarosik, D. Larson, M. Limon, L. Page, et al., ApJS **180**, 330 (2009), 0803.0547.
- [45] N. Kaiser, H. Aussel, B. E. Burke, H. Boesgaard, K. Chambers, M. R. Chun, J. N. Heasley, K.-W. Hodapp, B. Hunt, R. Jedicke, et al., in *Society of Photo-Optical Instrumentation Engineers (SPIE) Conference Series*, edited by J. A. Tyson and S. Wolff (2002), vol. 4836 of *Presented at the Society of Photo-Optical Instrumentation Engineers (SPIE) Conference*, pp. 154–164.
- [46] J. A. Tyson, in *Society of Photo-Optical Instrumentation Engineers (SPIE) Conference Series*, edited by J. A. Tyson and S. Wolff (2002), vol. 4836 of *Presented at the Society of Photo-Optical Instrumentation Engineers (SPIE) Conference*, pp. 10–20.
- [47] LSST Science Collaborations, arXiv:0912.0201 (2009), 0912.0201.
- [48] H. Zhan, L. Wang, P. Pinto, and J. A. Tyson, ApJ **675**, L1 (2008), 0801.3659.
- [49] M. Davis and P. J. E. Peebles, ApJS **34**, 425 (1977).
- [50] M. E. C. Swanson, M. Tegmark, M. Blanton, and I. Zehavi, MNRAS **385**, 1635 (2008), arXiv:astro-ph/0702584.
- [51] D. W. Hogg, ArXiv Astrophysics e-prints (1999), arXiv:astro-ph/9905116.
- [52] P. A. Pinto, C. R. Smith, and P. M. Garnavich, in *Bulletin of the American Astronomical Society* (2004), vol. 36 of *Bulletin of the American Astronomical Society*, pp. 1530–+.
- [53] J. Estrada, E. Sefusatti, and J. A. Frieman, ApJ **692**, 265 (2009), 0801.3485.
- [54] F. Bernardeau, L. van Waerbeke, and Y. Mellier, A&A **322**, 1 (1997), arXiv:astro-ph/9609122.
- [55] P. Valageas, A&A **356**, 771 (2000), arXiv:astro-ph/9911336.
- [56] R. E. Smith, J. A. Peacock, A. Jenkins, S. D. M. White, C. S. Frenk, F. R. Pearce, P. A. Thomas, G. Efstathiou, and H. M. P. Couchman, MNRAS **341**, 1311 (2003), arXiv:astro-ph/0207664.

- [57] D. J. Schlegel, C. Bebek, H. Heetderks, S. Ho, M. Lampton, M. Levi, N. Mostek, N. Padmanabhan, S. Perlmutter, N. Roe, et al., ArXiv e-prints (2009), 0904.0468.
- [58] W. L. Freedman, B. F. Madore, B. K. Gibson, L. Ferrarese, D. D. Kelson, S. Sakai, J. R. Mould, R. C. Kennicutt, Jr., H. C. Ford, J. A. Graham, et al., *ApJ* **553**, 47 (2001), arXiv:astro-ph/0012376.
- [59] D. Huterer, A. Kim, L. M. Krauss, and T. Broderick, *ApJ* **615**, 595 (2004), arXiv:astro-ph/0402002.
- [60] A. G. Riess, L. Macri, S. Casertano, M. Sosey, H. Lampeitl, H. C. Ferguson, A. V. Filippenko, S. W. Jha, W. Li, R. Chornock, et al., *ApJ* **699**, 539 (2009), 0905.0695.
- [61] W. J. Percival, B. A. Reid, D. J. Eisenstein, N. A. Bahcall, T. Budavari, J. A. Frieman, M. Fukugita, J. E. Gunn, Ž. Ivezić, G. R. Knapp, et al., *MNRAS* **401**, 2148 (2010), 0907.1660.
- [62] E. Komatsu, K. M. Smith, J. Dunkley, C. L. Bennett, B. Gold, G. Hinshaw, N. Jarosik, D. Larson, M. R.olta, L. Page, et al., ArXiv e-prints (2010), 1001.4538.
- [63] A. P. Hearin, A. R. Zentner, Z. Ma, and D. Huterer, arXiv:1002.3383 (2010), 1002.3383.
- [64] B. Jain and P. Zhang, *Phys. Rev. D* **78**, 063503 (2008), 0709.2375.
- [65] W. Hu and I. Sawicki, *Phys. Rev. D* **76**, 104043 (2007), 0708.1190.
- [66] E. V. Linder, *Phys. Rev. D* **79**, 063519 (2009), 0901.0918.
- [67] R. Juszkiewicz, H. A. Feldman, J. N. Fry, and A. H. Jaffe, *JCAP* **2**, 21 (2010), 0901.0697.
- [68] G. Dvali, G. Gabadadze, and M. Porrati, *Physics Letters B* **485**, 208 (2000), arXiv:hep-th/0005016.
- [69] C. K. McBride, A. J. Connolly, J. P. Gardner, R. Scranton, R. Scoccimarro, A. A. Berlind, F. Marin, and D. P. Schneider, ArXiv e-prints (2010), 1012.3462.
- [70] L. Verde, A. F. Heavens, W. J. Percival, S. Matarrese, C. M. Baugh, J. Bland-Hawthorn, T. Bridges, R. Cannon, S. Cole, M. Colless, et al., *MNRAS* **335**, 432 (2002), arXiv:astro-ph/0112161.

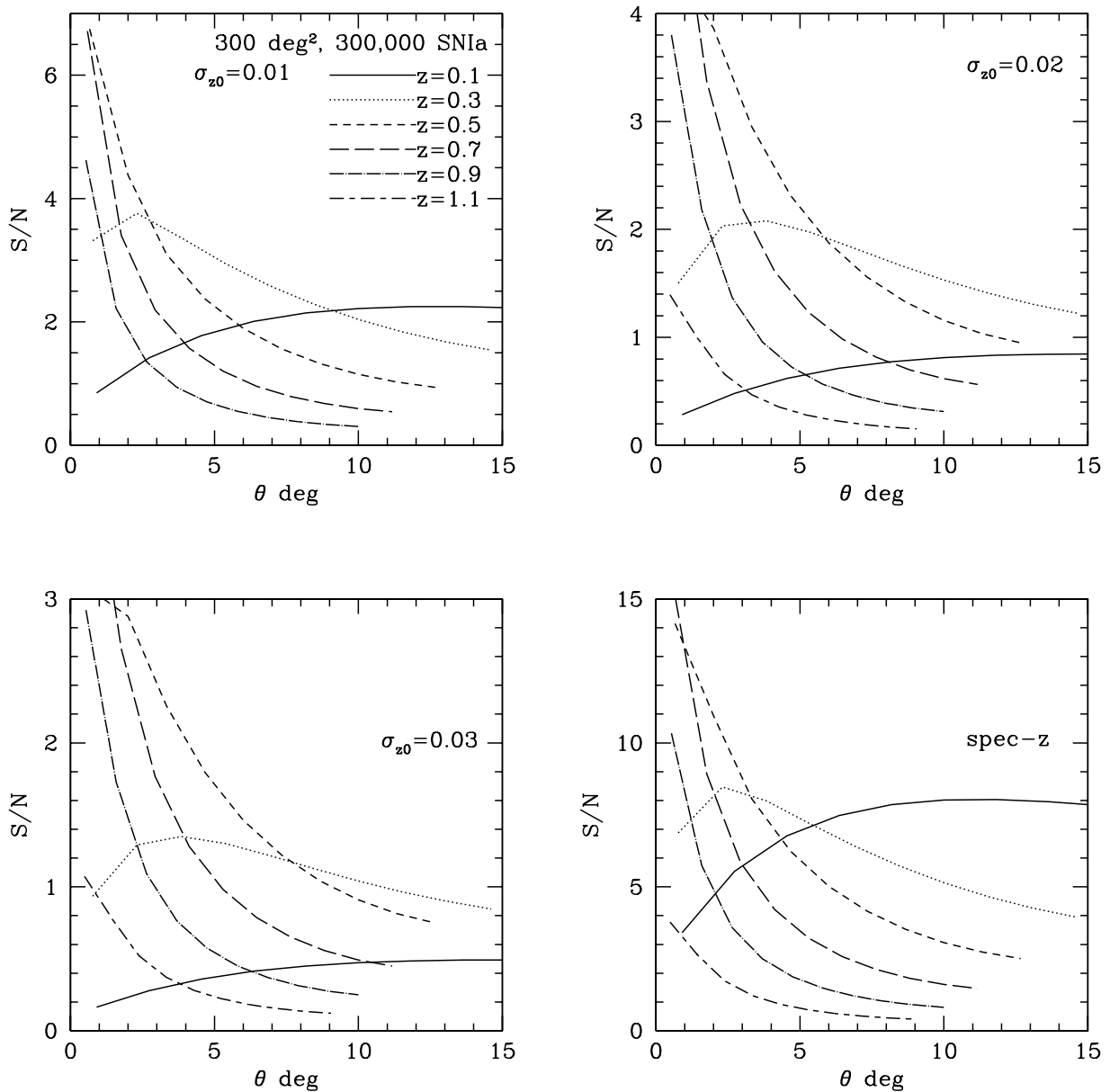


FIG. 2: The signal-to-noise per angular bin for the projected mean pairwise velocity for different redshift bins as a function of angular separation  $\theta$ , for a catalog with  $3 \times 10^5$  total host galaxies over 300 square degrees of sky, and a distance modulus scatter for each host galaxy of  $\sigma_{\text{SN}} = 0.1$  plus the scatter due to lensing magnification. The pairs are binned by their photometric redshifts and the central values of the redshift bins are shown; each redshift bin has a width of  $\Delta z = 0.2$ . The maximum angle for each redshift bin corresponds to the angle subtended by 100 Mpc at the bin’s mean redshift; the range in angles from 0 to the maximum angle is divided into 10 angular bins. The top panels show the signal-to-noise for a photo- $z$  normal error given by  $\sigma_z = \sigma_{z0}(1+z)$ , where  $\sigma_{z0} = 0.01$  (left) and  $\sigma_{z0} = 0.02$  (right). The lower left (right) panel shows the signal-to-noise for  $\sigma_{z0} = 0.03$  (left) and the “spectroscopic” limit with  $\sigma_{z0} = 0.001$  (right).

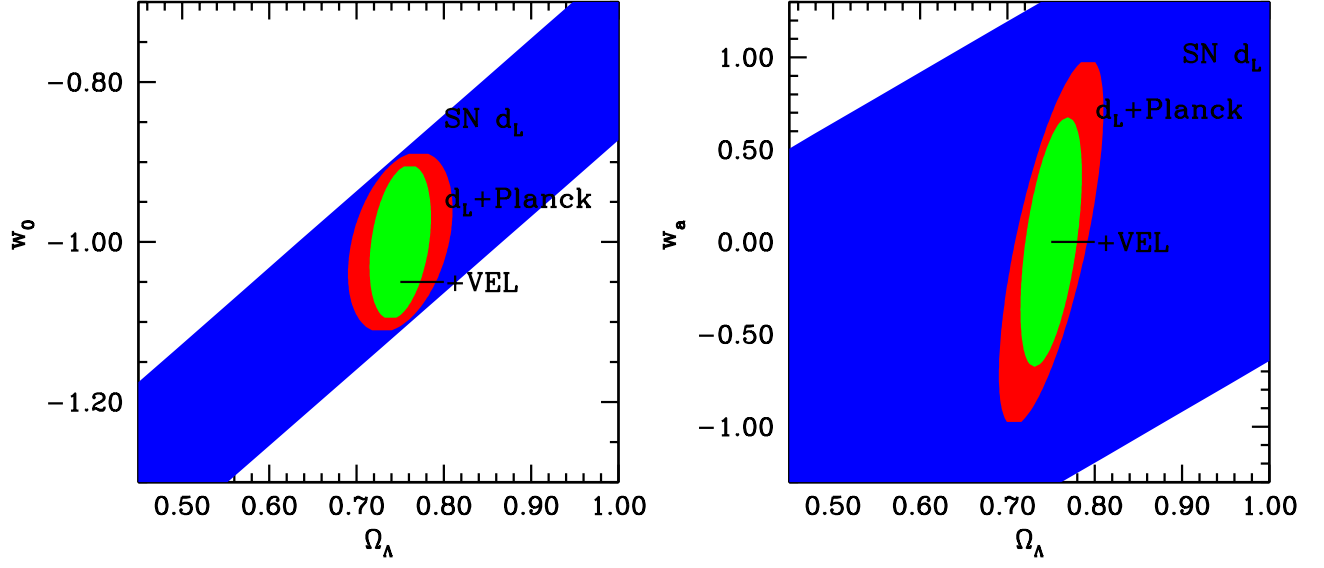


FIG. 3: Joint dark energy constraints obtainable from an LSST-like future supernova survey, combining constraints from the supernovae luminosity distance test, priors on Hubble parameter [58] and constraints from Planck with those obtainable from supernova velocity statistics. A flat universe is not assumed. A fiducial value for the photometric redshift error of  $\sigma_{z_0} = 0.01$  is assumed, with a Gaussian prior on  $\sigma_{z_0}$  of 5%. The Fisher matrices for the Planck priors and the SNIa luminosity distance priors are obtained from the DETF report [43]. The luminosity distance Fisher matrix represents the DETF LSST supernovae optimistic (LST-o) survey. The blue (dark) shaded region shows the constraint obtainable from the supernova luminosity distance test only. The red (grey) region shows the constraint when priors from a Planck survey are combined with the distance test. The green (innermost, light shaded) region shows the joint constraint combining the distance test, a Planck prior and mean peculiar velocity measurements for the SNIa host galaxies.

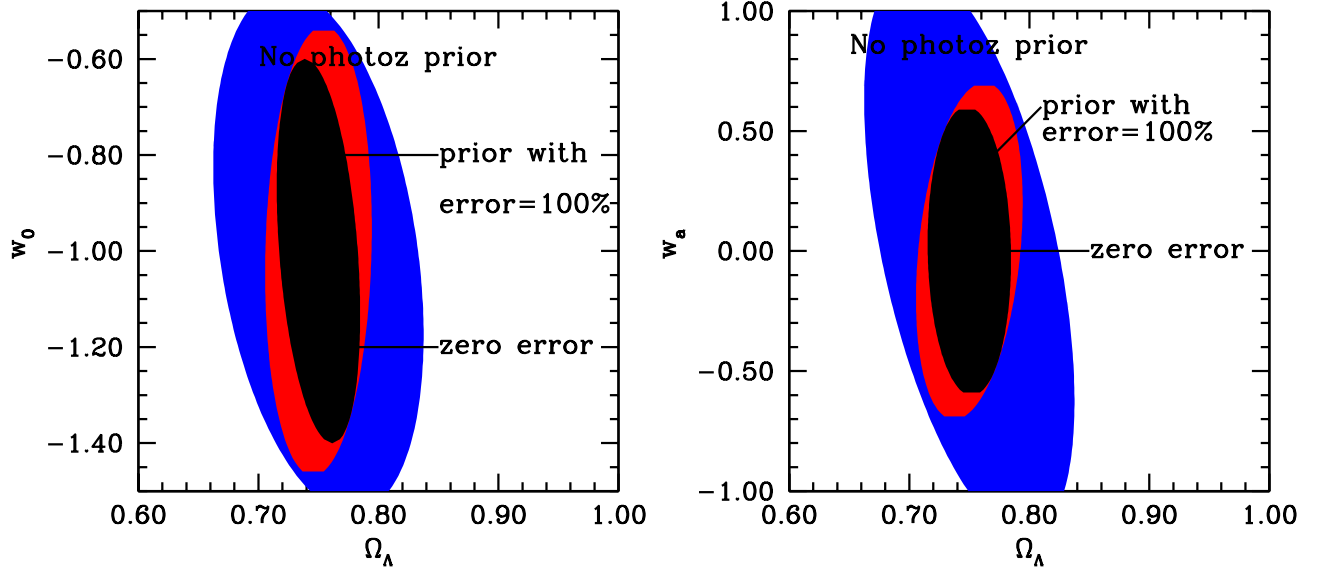


FIG. 4: Dark energy parameter constraints from mean pairwise SNIa velocities (in the absence of complementary cosmological probes), for the same survey as in Fig. 2. The left and the right panels show the  $1\sigma$  contour in the  $w_0 - \Omega_\Lambda$  and the  $w_a - \Omega_\Lambda$  planes. Photometric redshift errors of  $\sigma_z = 0.01(1+z)$  are assumed. The black shaded region represents the case when the photo- $z$  distribution is known accurately. The red (light shaded) region applies a prior such that the uncertainty in the photometric redshift error,  $\delta\sigma_{z0}$ , is equal to the value of  $\sigma_{z0}$ ; this is highly conservative. The blue (gray) shaded region shows the constraint when we have no prior knowledge about the photo- $z$  error distribution (e.g., zero supernovae with spectroscopic redshifts).